Morphological characterization of landforms produced by springtime seasonal activity on Russell Crater megadune, Mars

Gwenaël Jouannic, Susan J. Conway, Julien Gargani, F. Costard, Marion Massé, Olivier Bourgeois, John Carter, Frédéric Schmidt, Chiara Marmo, Gian Ori, et al.

Morphological characterisation of landforms produced by springtime seasonal activity on Russell Crater megadune, Mars

Gwenaël Jouannic[1, 2, *], Susan J. Conway[3], Julien Gargani[1], François Costard[1], Marion Massé[3], Olivier Bourgeois[3], John Carter[4], Frédéric Schmidt[1], Chiara Marmo[1], Gian G. Ori[5,6], Marion Nachon[7], Kelly Pasquon[1]

1 Work done at GEOPS, Université Paris-Sud and CNRS, Bât. 509, 91405 Orsay, France.

2 Now at Cerema, Département Ville et Territoire, 9 rue Viviane, BP 46223 - 44262 Nantes cedex 2, France.

3 Laboratoire de Planétologie et Géodynamique, CNRS UMR 6112, Université de Nantes, 2 chemin de la Houssinière, BP 92205, 44322 Nantes Cedex 3, France.

4 IAS, Université Paris-Sud and CNRS, 91405 Orsay, France.

5 International Research School of Planetary Sciences, Università "G. d'Annunzio", Viale Pindaro 42, 65127 Pescara, Italy.

6 Ibn Battuta Centre, Université Cady Ayyad, Marrakech, Morocco.

7 University of California Davis, Earth and Planetary Sciences, Davis, CA 95616, USA

* Correspondence to: gwenael.jouannic@cerema.fr

Abbreviated title: Seasonal activity on Russell Crater megadune

Abstract

We describe in detail an annual seasonal process that occurs on the surface of the Russell Crater megadune on Mars. We give these features the name ‘perennial rills’, because their surface topographic expression persists from year-to-year and they form a distinctive, downstream branching network of small channels, or rills. We used time series images, elevation data from stereo photogrammetry and spectral data to characterise the evolution of these features over six Mars Years. Growth and modification of these networks occurs abruptly in spring (at approx. solar longitude 200°) after most of the seasonal CO_2 ice has sublimated. We find that the peculiar morphology of perennial rills seems to be the only aspect that sets them apart from active linear dune gullies. By comparison to terrestrial analogues we identified two conditions favouring the production such a network: a) the presence of an impermeable layer and b) the repeated formation of obstacles in front of propagating channels. We find that the most plausible formation mechanisms that can explain the formation of both the perennial rills and active linear dune gullies are levitating CO_2 blocks, or liquid debris flows of water/brine, but neither can completely satisfy all the observational evidence.

Keywords: Mars; water; ice; sediment transport; martian gullies; CO_2; seasonal processes

Active martian surface processes that are linked to the seasonal cycle are responsible for the most prevalent surface changes observed over recent decades and their origin is heavily debated. Repeat imaging by high resolution (better than 10 m/pix) sensors has enabled us to investigate how martian surface features evolve with time and assess their intra-annual variability. Seasonal processes result in surface changes that are small in scale (tens to hundreds of metres) and although the majority only leave ephemeral visual traces some cause measurable topographic change (e.g. spider-like-forms, Piqueux et al., 2003). Seasonal processes acting on dark martian sand dunes are particularly active and they have a wide range of timings and morphologies. These include: formation and extension/modification of gully-channels, alcoves and fans, formation of pits, appearance/evolution of ephemeral dark spots/flows with or without bright halos, and formation of dust devil tracks (e.g., Pasquon et al., 2016, 2018). This study focuses on a phenomenon that was first noticed by Reiss et al. (2010a) on the Russell Crater megadune (Fig. 1; 54.5°S; 12.7°E), and here we report on its annual recurrence and detail its morphology. This phenomenon occurs during spring and is characterised by the abrupt appearance of a network of distributary narrow depressions, or channels, which extend downslope. We use the term 'perennial rills' to distinguish this landform from other seasonal landforms (Fig. 2) that also appear on the Russell Crater megadune. These perennial rills form on and between the large linear dune gullies, which densely cover the megadune's lee slope (Fig. 3). We use the term perennial, because they persist for one or more Mars Year.

With the exceptions of dust devil tracks, seasonal processes on dunes have been directly linked to the annual extension and recession of the seasonal ice-deposits, which extend downwards from the poles (continuously to ~50° latitude; e.g., Piqueux et al., 2015). These deposits develop over winter, with a relatively small amount of water-ice being laid down first, followed by CO_2 ice (Ivanov and Muhleman, 2001). The CO_2 ice is estimated to be ~0.5 m thick

at the latitude of Russell Crater (Cull et al., 2010; Smith et al., 2001) and is thought to metamorphose into translucent slab-ice during autumn/winter. In the winter/spring this ice cover regresses towards the pole, with first the sublimation of CO_2 ice, followed by the sublimation of H_2O ice (e.g., Bapst et al., 2015). The sublimation of CO_2 ice is one of the explanations proposed for the formation of dark spots and dark flows that appear on the surface of dunes covered with seasonal CO_2 ice (Piqueux et al. 2003; Kieffer et al., 2006; Kieffer, 2007; Hansen et al. 2011, 2013; Gardin et al., 2010). However, other mechanisms have also been proposed for the formation of these features, including the development of a centimetre-to-decimetre thick layer of temporary liquid sub-surface water or brines (Möhlmann, 2010; Kereszturi et al., 2011b).

The aims of this study are 1) to characterize the morphology of the perennial rills and how they evolve with time, 2) to document their evolution in context with the other seasonal processes on the dune, 3) to identify potential terrestrial analogues in order to place constraints on their formation, in order to determine whether and how their formation is linked with the seasonal ices and with the (presumably) longer term evolution of the linear dune gullies on the Russell Crater megadune.

Study area

This study area is located on the megadune which is found within a dunefield on the floor of Russell Crater (54.5°S, 12.7°E; see Fig. 1). The megadune is about 36 km long, 10 km wide and 500 m high and has been formed by aeolian transport and deposition (Gardin et al., 2010). The major constituent of the dark sand-sized sediments forming dunes on Mars is thought to be pyroxene with some olivine (e.g., Achilles et al., 2017; Tirsch et al., 2011), probably detrital minerals of volcanic origin. The pole-facing western lee slope has an average slope of 10° (Reiss

et al. 2010a) and more than 300 “linear” dune gullies are visible on this face (Reiss and Jaumann, 2003). No gullies are observed on the gentler stoss slope to the east which has a mean slope of 5°. Linear dune gullies are a particular sub-class of martian gullies that have a distinct morphology (Diniega, 2014) and are found not only on sand dunes, but also on other sand-covered slopes (Auld and Dixon, 2016). These gullies comprise a relatively small (compared to their overall length) tributary source area, an extremely long, almost constant-width channel (extending almost the whole slope-length) following the direction of the slope and an abrupt terminus, often associated with terminal pits (Jouannic et al., 2012; Pasquon et al., 2016). The preferential orientation of linear gullies on S-SW flanks is thought to be related to insolation processes (e.g. Balme et al., 2006 ; Pasquon et al., 2016), but could also be related to the restriction of gullies to steep slopes (e.g., Conway et al., 2017).

The linear dune gullies on the Russell Crater megadune are known to undergo seasonal changes including: 1) linear gully growth/extension, including formation of pits, 2) development of dark-spots and dark-flows, 3) appearance of bright halos, 4) formation and erasure of dust devil tracks and 5) development of perennial rills, which are the focus of this study. Previous work on these phenomena will be outlined in the following sections.

Summary of previous work on seasonal processes on dunes

Gully modifications

Linear dune gullies are a sub-class of martian gullies (Conway et al. 2018) composed of a relatively long and narrow channel, with a relatively restricted alcove and terminal deposits (on the Russell Crater meagdune they can be ~2 km long for ~10 m wide). They are found in 33 dune-filled craters - Russell Crater included – exclusively in the southern hemisphere (Pasquon et

al., 2016) and represent ~4.8% of the total number of gully sites (Auld and Dixon, 2016). The channel is often perched in the downstream part and lateral levees of ~1 m can be observed (Jouannic et al., 2015). The linear dune gullies on the Russell Crater megadune are the largest known, probably because the Russell megadune is the largest dune on which such gullies are found. Recent changes observed in the linear gullies on the Russell Crater megadune include channel extension and reworking, as well as CO_2 frost evolution in the gully channel (Reiss et al., 2010a). Dundas et al. (2012) reported on the appearance of bright "blocks" in linear dune gully channels contemporaneously with the gully modifications. Recent activity of linear dune gullies has been observed in 53% of the sites where they occur (Pasquon et al., 2016). Active linear dune gullies can lengthen by ~100 m per Mars Year between the end of winter and the beginning of spring (L_s 167.4°-216.6°, where L_s stands for Solar Longitude, which describes the position of Mars in its orbit around the Sun, i.e., the seasons). This growth coincides spatially, as well as temporally, with the appearance of digitate-shaped, dark patches (whose albedo is low compared to the surrounding terrain) that encompass the active gully site – termed "Recurring Diffusing Flows" (RDF; Pasquon et al., 2016). These modifications occur on south-southwest facing slopes with a mean slope of 13.9°, and where the slope just below the crest is >20° (Pasquon et al., 2016). CO_2 frost sublimation (Dundas et al., 2012; Dundas et al., 2015) and CO_2 driven dry processes (Diniega et al., 2010; Diniega et al., 2013) have been suggested to be the cause of these recent modifications in martian dune gullies, because the modifications always coincide with the end of the CO_2 defrosting period. However, because the exact mechanism producing these changes remains elusive, other processes particularly those involving the production of small amounts of liquid water are still under consideration (Pasquon et al., 2016, 2018).

Dark spots and dark flows

Various seasonal low albedo features have been previously identified on the relatively high albedo frosted dune surfaces of the polar regions of Mars. These features can be divided in two morphologic groups: dark spots, including those associated with spider-like structures (e.g., Christensen et al., 2005; Kieffer et al, 2006; Kossacki and Kopystynski, 2004; Malin et al., 1998; Piqueux et al., 2003; Hansen et al. 2010, Thomas et al. 2010) and dark flow-like features (Kereszturi et al., 2009; Kereszturi et al., 2010; Gardin et al., 2010; Möhlmann, 2010; Raack et al., 2015). Dark spots are low albedo circular to oblate patches, which tend to grow and coalesce with time (Fig. 2c). Dark flows often initially look like dark spots, but later develop into elongate digitate structures, which stretch downhill, sometimes following ripple-furrows (Fig. 2b). Both are tens to hundreds of metres in size. Two processes have been proposed to explain the formation of these features on dunes: 1) a centimetre-to-decimetre thick layer of temporary liquid sub-surface water or brines (Möhlmann, 2010, 2011; Kereszturi et al., 2011b); 2) a geyser-process triggered by the basal sublimation of seasonal CO_2 ice-slab whereby CO_2 gas, dust and sand erupt from underneath the slab-ice and avalanche down the slope of dunes (Piqueux et al. 2003; Kieffer et al., 2006; Kieffer, 2007; Gardin et al., 2010). The dark spots and dark flows on the Russell Crater megadune were previously described by Gardin et al. (2010) and occur during winter, nucleating on positive topography and bright cracks in the CO_2 slab-ice. These dark features (spots and flows) are generally aligned along cracks, in particular on the steeper slopes of the megadune. Gardin et al. (2010) estimated that these kinds of flows transport in the order of 0.25 to 0.5 m^3 per metre width per year. Hence, the volume of material mobilised over the course of a single year by this transport process would be undetectable, even at the best imaging resolution of 25-50 cm/pixel.

Bright halos

The dark flows are sometimes surrounded by a bright halo, which has higher albedo than the dark flow and the surrounding terrain (Fig. 2d), in previous work these were also termed “white collars” (Kereszturi et al., 2010 ; Kereszturi et al., 2011b ; Möhlmann, 2010). Previous studies have reported the presence of bright halos around dark spots on dunes in general in the southern hemisphere (Kereszturi et al., 2009). Kereszturi et al. (2011a) report that these halos have a CO_2 frost signature. They noted that bright halos emerge immediately after the disappearance of the dark flows and dark spots, when the temperature is above 170 K in Russell Crater (Kereszturi et al., 2011b). These bright haloes have also been associated with the RDF that surround active gully sites (Pasquon et al. 2016).

Dust devil tracks

Dust devils are low pressure vortices, found on both Earth and Mars (e.g., Greeley et al. 2005; Reiss et al., 2010b, 2011b). The first active dust devils were identified on Mars in Viking orbiter images (Thomas and Gierasch, 1985). These spiralling vortices are caused by heating of near-surface air by insolation. They transport small particles such as dust and fine sand, and are suggested to be responsible for a significant part of the dust transport on Mars (Balme and Greeley, 2006). They are a common active process on Mars (e.g., Balme and Greeley, 2006; Cantor et al., 2006; Fisher et al., 2005; Malin and Edgett, 2001; Reiss et al., 2011a; Stanzel et al., 2006) and change the surface albedo by removing dust (Neakrase et al. 2016) and forming curving tracks on the surface (Fig. 2e). Dust devil tracks are not reported on surfaces where, and

at times of year when, the seasonal ice is present. Their tracks can be used as an indicator of when the seasonal ices have completely sublimated from a surface.

Materials and methods

Using 87 High Resolution Imaging Science Experiment (HiRISE, 25 - 50 cm/pix) images (Table 1) over a 125 month period (November 2006 - April 2017; Mars Years 28 - 33), we followed the evolution of the surface of the Russell Crater megadune over time. We applied the same Transverse Mercator projection centred on 13°E to all HiRISE images, and manually refined the metre-scale co-alignment between the images. For non-nadir images we used an ortho-rectified or nadir image as a reference and then by using a network of 10-20 control points we manually corrected for the topographic distortion. Areas and lengths of features were measured directly from shapes digitised onto the HiRISE images in ArcGIS. To estimate the growth rate of different seasonal process with time we mapped all of the features on subsequent HiRISE images (as in Ceamanos et al., 2011) for the first three Mars Years. The change in area was divided by the time interval between images, to determine a growth rate. In order to allow comparison between seasonal processes the results were normalised by the overall area affected by the process.

We made a plan view map of the rills making up the perennial rill network for the 5 Mars Years of observations, digitising each rill as a polyline feature in the first springtime image where these features appear. To quantify how the density of the rill network changed with time we calculated the fractal dimension of the polyline network digitised from the images as follows. The statistical number-size distribution for a geomorphic feature can be scale invariant and in other words fractal. For the distribution to be fractal, the number of line segments N with a

202 characteristic linear dimension greater than *r* should satisfy the relation $N = C/r^D$ where *D* is the
203 fractal dimension (Turcotte, 1997) and *C* a constant. This method allowed us to characterize the
204 spatial density and the scale invariance of the perennial rills. The fractal dimension of the
205 perennial rills was calculated using the box counting method of Turcotte (1997), whereby a
206 square mesh with a spacing of *r* is superposed onto the rill systems. *N* was determined by
207 counting the number of boxes which contain rills. This manipulation was performed in ArcGIS
208 by using the feature to raster tool with output cellsizes of 0.5, 0.75, 1.0, 1.5, 2.0, 2.5, 5.0, and
209 10 m and then counting the number of cells with data. *N* was then plotted on a log-log diagram
210 against the grid-scale *r* and a linear regression performed to ascertain the fractal dimension.
211 Sinuosity of line-features was calculated by taking the ratio of the length of the trace to the
212 straight-line end-to-end length.
213 We analysed one HiRISE and one HRSC (High Resolution Stereo Camera) DTM (Digital
214 Terrain Model) using the 3D analyst tools of ArcGIS software in order to estimate the value of
215 the slope in the different areas of interest. The HRSC data (H2247_0000) were level 4 HRSC
216 elevation data acquired from ESA's Planetary Science Archive (Scholten et al., 2005) with a
217 resolution of 75 m/pix. The HiRISE elevation data were derived from the stereo-pair
218 PSP_007018_1255 and PSP_007229_1255 using the methods described by Kirk et al. (2008) and
219 we estimate the vertical precision of this DTM to be ~0.62m. This DTM was produced by the
220 authors of Jouannic et al. (2012), where details on its production and precision can be found.
221 Absolute deviation of the HRSC elevation data from the MOLA (Mars Orbiter Laser Altimeter)
222 spot heights is reported to be on the order of 29 m with a standard deviation of 41 m (Gwinner et
223 al., 2009).
224 We performed a spectral analysis to determine the mineralogical surface composition.
225 CRISM suffers from high noise levels and multiple non-stochastic instrument artefacts in the

spectral and spatial domains. The sources of biases were overcome by using a standard set of corrections that remove the instrument artefacts, the contaminating minerals and photometric effects as described in Carter et al. (2013). Spectra from the corrected CRISM data were compared to the entries in the RELAB spectral repository and Hanley et al. (2011) to ascertain potential surface composition. Mapping of the identified minerals was undertaken in ENVI. We analysed CRISM data FRT00005339 acquired at L_s = 215° during Mars Year 28.

Observations of perennial rills

In the following sections we divide our observations into three parts. Firstly, we present the morphology of the perennial rills, secondly we present the changes observed in these features over time, and thirdly we present our observations on the timing and distribution of the other seasonal processes on Russell Crater megadune and place the perennial rills into this context.

Perennial rill morphology

The perennial rills are located on portions of the southwest-facing lee slope of the Russell Crater megadune (Fig. 3). The perennial rills are usually found between ~200 m and 1000 m from the crest of Russell Crater megadune (Fig. 3) with three small networks located at the termini of existing linear dune gullies 3500 m from the dune crest. We assign each discrete perennial rill system with a “Zone” which encompasses the total area affected by the system over the five MY covered by this study. We identified 28 zones with active perennial rill systems. Each system comprises a distributary system formed by numerous small branching, sinuous rills (sinuosity index is ~1.1; Figs. 4 and 5). Their branching angles are typically ~ 45° and their direction deviates from directly downslope (Fig. 5). The system of perennial rills which is located closest

to the dune crest (Zone 1) has a mean slope of ~12° (Fig. 3) and the other systems have lower slopes, because they are located further down the lee slope. The maximum width of these small channels is ~1 m without observable symmetric lateral deposits (levees). A zone with a lower albedo than the surrounding dune (from here on termed the "dark zone") extends over and slightly beyond the area affected by the perennial rills (Figs.3, 4 and 5). This dark zone appears at the same time as the new generation of perennial rills. Both the perennial rills and these dark zones originate from linear dune gully channels, connecting to the southern edge of a channel (with multiple rills breaching any given gully channel wall), or fanning out from linear dune gully channel termini (three such systems are located at the base of the slope and three mid-slope).

The 1 m/pix resolution of the HiRISE elevation data are insufficient to directly confirm that the rills cause topographic change. Shadow measurements cannot be used, because no distinct shadow-edge can be identified in the images. The rills are not wide enough to have a distinct shadow cast on their floor by their walls, because their width is near the image resolution. Nevertheless, the topographic expression of the rills can be inferred from the HiRISE images at 25 cm/pixel, using the following arguments: a) independent of the time of year the rills are picked out by light-dark-light patterns in the images implying topographic shadowing, unrelated to the distribution of seasonal ices, and b) relict rills, which are not reactivated the following year are partially filled with aeolian ripples suggesting a topographic trap (Fig. 5). Using the plan-dimensions of the rills alone we can make a reasonable estimate their depth. The width of the perennial rills is ~1 m and it is reasonable to assume that the depth of the rills is not greater than their width. In addition, given that the angle of repose for loose sand is ~30° on Mars (Atwood-Stone and McEwen, 2013), hence the maximum depth of the rills should be ~0.3 m, but is likely to be less.

Changes observed in perennial rills

The appearance of a new perennial rill system, or evolution of an existing system occurs abruptly between L_s 183° and 221° in each Mars Year for which we have observations (MY 28-33) and this is detailed further below. During the six Mars Years we observed the formation of 5 new perennial rill systems >500 m long and 23 smaller systems (Table 2). Mars Years 32 and 33 were most active both in terms of approximate surface area which underwent changes and in terms of number of perennial rill systems that were active (Table 2). We only observed one system >500 m long that was active in all Mars Years (Zone 1).

In the following sections we describe in detail each of the different changes (listed as a-e below) observed in these rills systems, and we use Zone 1 as the case study to illustrate these changes:

a) Growth of the area affected by the rill system and its associated dark zone;
b) Re-use and extension of individual rills;
c) Creation of new rills, either overprinting an older network or onto an unaffected dune surface;
d) Disappearance of rills; and
e) Stability of the network density from year-to-year.

Growth of the area affected by the rill system

The size of the dark zone surrounding the perennial rills in Zone 1 grew over Mars Years 28-30 by ~22 000 m^2 and in MY31 only changed slightly and decreased by 10 000 m^2 in MY32 having the same area but different shape in MY33 (see Figs. 4 and 5). This sudden growth behaviour is

also shown by Zone 2 (to the left of Zone 1 in Fig. 3) which between MY30 and 31 extends from ~40 m to ~400 m in length (350 m extension), further extending by 130 m in MY32 and 30 m in MY33. We did not note any fading of the dark zones in the summer that followed their appearance, but if a dark zone is not renewed then it appears faded after the frost has sublimated the following Mars Year.

Re-use and extension of rills

In the upper part of the perennial rill systems we observe that the same rills tend to persist from year to year (Figs.6b1, 6b2 and 6b3). These rills widen each year, increasing in width by 1 to ~4 m between MY 28 and 30. An example of rill-extension is shown in Fig.5. The rill marked with an arrow is confined within a partly infilled larger gully channel. In Mars Year 28, this rill lengthened downslope by about 86 m (Fig.5a), an extension previously observed by Reiss et al. (2010a). In Mars Year 29, it further lengthened by ~ 145 m (Fig.5b) and in Mars Year 30 it lengthened by ~190 m (Fig.5c). Another, less dramatic example is shown in Figs. 5g-i, where a rill lengthens several tens of metres each Mars Year. In this example the rill extends through the formation of new smaller rills at its terminus which diverge and extend downslope.

Creation of new rills

The majority of the new rills occur in the lower and distal part of an existing perennial rill system (Figs.5d,-i), where we observe new rills and a resultant increase in sinuosity from year-to-year. Here, new rills are easily identified, because they extend over previously unaffected surfaces of the dune. Higher in the network only a few new rills appear (Figs.6b1, 6b2 and 6b3). These new rills are in general shorter and narrower than the rills that have persisted over one or more Mars

Years. The new rills are ~1 m wide with a sinuosity index > 1.1 and the established rills are 1-5 m width with a sinuosity index < 1.05. Sometimes whole networks spontaneously appear on the dune surface without any apparent pre-existing network (e.g., Zone 15, Table 2).

Disappearance of rills

In the lower part of the system, the smaller rills are gradually overprinted and can be erased by the extension of upslope rills during a new phase of activity (Figs.4, 5d-i). Rills can also disappear without being overprinted (Figs.5g and 5h): the sinuous channels are gradually transformed into ripples which are continuous with those found on the rest of the lee slope. This transition is gradual (taking more than one Mars Year generally) and may also be aided by mass wasting into the channel, or frost-driven processes, however no specific evidence is found either for or against these additional processes.

Density of rills

The majority of the rills that make up the main branches of the rill systems are preserved from one year to the next, but as highlighted above the topology of the network changes over time. The fractal dimension of the perennial rill system ranges from D = 1.132 to D = 1.209 (Fig. 7). Unlike the growth, the density of the network has no particular trend over time and its fractal nature is preserved.

Timing, growth rate, and distribution of seasonal processes and perennial rills

Dark spots

The dark spots (Fig. 2c) are located on the low- and mid-slope parts of the Russell Crater megadune lee slope, where slopes range from 2° to 24° with a mean of 10°. We observed that when the slope is steeper, the dark spots are more extensive and more elongated (Figs. 8c1-8c6, the slope is steeper on the top-left compared to the bottom-right of this image). The diameter of the dark spots increases during winter (Fig. 8). They can reach a maximum diameter of ~30 m. We observed the preferential formation of dark spots on the north-westward oriented flank of the gully-channels. At the end of winter, most of the north-west-facing channel flanks have a dark appearance, which could be due to the coalescence of dark spots (Figs. 8c1-8c6), or could be a result of the removal of the CO_2 frost. Their first appearance is at L_s 115-136° (Fig. 9; Table 1). The first image without dark spots is taken in early spring between L_s 206° and 221° (Figs. 8c6 and 9). During the first period of winter (L_s 158° to 179°), the growth rate of dark spots was 1.7 x 10^{-8} $m^2.s^{-1}.m^{-2}$ (i.e. a growth rate of 7.2 x 10^{-2} $m^2.s^{-1}$ over a total area of 4.3 x 10^6 m^2), then it increases at the end of winter (L_s 179° to 182°) to reach 3.2 x 10^{-8} $m^2.s^{-1}.m^{-2}$ (i.e. a growth rate of 1.4 x 10^{-1} $m^2.s^{-1}$ over a total area of 4.3 x 10^6 m^2).

Dark flows

The dark flows (Fig. 2b) are located on steeper terrain than the dark spots. They are found on the first 200 m under the crest of the Russell megadune where the slope ranges from 12° to 28° (Fig. 3) with a mean slope of 19° (Figs. 8b1-8b6). Initially dark flows and dark spots have a similar morphology (Fig. 8b2), but some dark spots evolve into dark flows (Figs. 8b3-8b5), which become channelised between the aeolian ripples of the megadune, as described by Gardin et al. (2010). The length and width of the dark flows increases during winter (Fig. 8). We found that the dark flows appear later than the dark spots at around L_s 159-176° (Table 1). The first image

without dark spots and dark flows is taken in early spring between L_s 206° and 221° (Figs. 8b6 and 8c6, Fig. 9). During the first period of winter (L_s 158° to 179°), the growth rate of dark flows is 4.2 x 10^{-8} $m^2.s^{-1}.m^{-2}$ (i.e. a growth rate of 1.2 x 10^{-2} $m^2.s^{-1}$ over a total area of 2.8 x 10^5 m^2), then it increases at the end of winter (L_s 179° to 182°) to reach 7.8 $m^2.s^{-1}.m^{-2}$ (i.e. a growth rate of 2.2 x 10^{-2} $m^2.s^{-1}$ over a total area of 2.8 x 10^5 m^2).

Bright halos

Bright halos (Fig. 2d) appear during early spring from L_s 177° to 221° (Fig. 9, Table 1) and they appear both around the perennial rills and other dark flows. They occur only on the steepest (from 12° to 28°) south-facing slopes. Bright halos typically appear on the image immediately following the last image with dark flows and dark spots, with one exception in MY33 where they appear on the same image. These halos are only visible in a single image each year, so we were not able to ascertain if they grow.

Dust devil tracks

On the Russell Crater megadune, dust devil tracks (Fig. 2e) have an average width of 38 m (ranging from 5 m to ~100 m), an average length of ~2.6 km and a mean sinuosity of ~1.3 (Verba et al., 2010). During spring and summer, many dust devil tracks are visible at the surface of the Russell Crater megadune (Figs. 8a1-8a6) between L_s ~200° and ~360° (Fig. 9, Table 1) with the maximum number visible at L_s ~316° (Verba et al., 2010). The number of dust devil tracks seems to increase sharply just after the complete sublimation of frost from the Russell Crater megadune, and then slowly decreases until the region is covered again in CO_2 frost (Figs. 8a1-8a6). We sometimes observed dust devil tracks during the spring defrosting period and they were located

exclusively on defrosted patches of the dune (e.g. north-facing slopes in early spring). Verba et al. (2010) showed that Global Climate Models predict prevailing north-westerly winds consistent with the dominant track direction in Russell Crater.

Relative timing of perennial rill activity and distribution

Table 1 provides a detailed breakdown of the HiRISE images used to constrain the timing of the activity in perennial rills and Table 2 details the activity of each rill system. In Mars Year 28, we noted the first series of changes in the perennial rill systems on the megadune's surface which occurred sometime between L_s 198° and L_s 218° (mid-spring) (Fig.5a). These changes in the Zone 1 rill system were previously briefly described by Reiss et al. (2010a). Considering the whole period between Mars Year 28 and 33 the changes observed in the perennial rill system occur in a tight L_s range, between 183° and 221° (Table 1; Fig. 9). Because the seasonal cap retreat is known to be very constant (Brown et al. 2010; Bapst et al., 2015; Piqueux et al., 2015) we can assume a negligible inter-annual variability, then rill-activity is most likely to occur between L_s 200° and 202°. This is at the end of the CO_2 defrosting period and coincides with the last observed dark spots and flows and the appearance of bright halos and the appearance of the majority of dust devil tracks (Table 1, Fig. 9). The fact that dust devil tracks are so numerous when the changes in the perennial rills occur attests to the fact that the majority of the surface of the megadune has already been defrosted at this point in time. Both the rill system and associated dark zone persist in the landscape after they first appear. The majority of the rill system persists through the whole year (sometimes even visible through the CO_2 frost in winter) until it is overprinted by the next generation of rill growth. The dark zone persists for the summer after its appearance and can sometimes be seen again the following spring if it is not overprinted. The

changes in the rills are not gradual or incremental, they occur suddenly between two images, the closest of which are only 6 sols apart (MY28, Table 1).

Using CRISM data Gardin et al. (2010) found that the last occurrence of seasonal CO_2 on Russell Crater's dunefield was between L_s 182 and 217° and HiRISE data reveal the last frost at L_s 197° was limited to the crest of the dune. From spectral data Reiss et al. (2010a) reported the last CO_2 signature at L_s 198°, with the first CO_2-free measurement at L_s 215°. From our study we noticed that the north-facing dune slopes defrosted first (at around L_s 140°), then the flat dune areas, then the south-facing slopes (progressing upwards from the base), with the steep crest of the south-facing slopes being the very last area to finally defrost, at around L_s 200° contemporaneously with the earliest observed appearance of the perennial rills (Fig. 4). From HiRISE data we cannot distinguish between CO_2 and H_2O ices.

Within the Russell Crater dunefield the perennial rills are restricted to discrete patches on the main megadune lee slope (Fig. 3). Compared to the other seasonal processes described here the extent of the perennial rills is localised, dark flows and spots occur continuously across large areas. The areal extent of the perennial rills totals between ~1.2×10^6 to 4.0×10^6 m^2 (Table 2) compared to 4.3×10^6 and 2.8×10^5 m^2 for dark spots and dark flows respectively and dust devil tracks can be found across the whole image.

Global Distribution of perennial rills and surface mineralogical content

The seasonal processes on the Russell Crater megadune also occur on other dunes on Mars. Hence, to assess whether there is a link between these seasonal processes (especially linear dune gullies) and the perennial rills, we inspected HiRISE images taken in spring for 32 dunefields located inside craters where linear dune gullies where observed by Pasquon et al. (2016). No

morphologies similar to perennial rills were observed on the surface of these dunefields, suggesting that the conditions required for perennial rill formation are rare and restricted to the Russell Crater megadune.

We identified hydrous minerals around the Russell Crater megadune in the interdune areas adjacent to the SW and NE flanks, as shown in Figure 10 (black spectra). The best laboratory matches to the CRISM spectra are a chloride hydrate, hydrated (opaline) silica, sulfates, zeolites and Al-smectites. Figure 10c shows a HiRISE close-up of the SW exposure. The hydrous minerals are found in a topographic low at the base of the dune, occurring mainly in association with the light-toned outcrops located at the base of numerous gullies, but signatures are also found on the neighbouring dark sand.

Discussion

Comparison between perennial rills and linear dune gullies

The perennial rill systems on the Russell Crater megadune are superimposed onto both the gullied and non-gullied part of the megadune lee slope. Hence, the rills are younger than the linear dune gullies. The perennial rills occur on the same lee slope as the linear dune gullies, but they are smaller in spatial extent and in scale. Although both form channel-like features on the dune surface, there are some notable morphologic differences between linear dune gullies and perennial rills.

The perennial rills are characterised by a highly connected distributary network of narrow (fractal dimension ranges from 1.147 to 1.209), sinuous channels (sinuosity is ~1.1). By contrast, the linear dune gullies on the Russell Crater megadune are relatively straight (sinuosity ranges from 1.01 to 1.06), parallel and generally occur as individual landforms rather than part of a

hierarchical network (Jouannic et al., 2012). The individual linear dune gullies have lengths of about 2 km, slopes ranging from 5° to 25° and widths between 3-20 m. Where linear dune gully-connections exist they form a tributary, rather than distributary configuration (Fig.5a). The distal reaches of perennial rill systems are dominated by a large number of distributary digitate rills resulting in an increase in the number of rills downslope (Figs.5d-i). By contrast, the number of linear dune gullies and their density decrease downslope due to the capture of tributaries by trunk channels.

Pasquon et al. (2016) found that changes in linear dune gullies and a phenomenon they termed Recurring Diffusing Flows (RDF) occur during late winter/early spring between L_s 167.4° and L_s 216.6° on Kaiser and Matara dunefields at 47°S and 50.5°S respectively. The timing of this activity coincides with the timing of changes in perennial rills. The changes they noticed included: the formation of new linear dune gullies, the extension of pre-existing channels and formation of new pits (Reiss et al., 2010). Similarly to the changes we observe in perennial rills, these gully-changes occur between two image acquisitions and were encompassed by a low albedo area that persisted after the changes had occurred (RDF). Pasquon et al. (2016) noted that RDF fade and can disappear from one year to the next, and they also noted that new linear dune gullies can be overprinted by ripples in few Mars Years after their creation if they are not reactivated, especially for those with lengths <150 m. These observations echo those for the dark zone around perennial rills and our observations on the disappearance of the perennial rill morphology if not reactivated. Pasquon et al. (2016) found linear dune gullies in Matara crater extended by 120 m (on average, 291 measurements) and up to 800 m, consistent with the extension in the largest perennial rill systems of ~350 m.

In contrast, the linear dune gully-changes noted by Pasquon et al. (2016) have a somewhat different position and morphology from the perennial rills described here. Changes in linear dune

gullies generally occur at the base of the lee slope (although some occur mid-slope), whereas the perennial rills occur predominantly towards the dune crest (Fig. 3). An important difference is the association between linear dune gully growth and the appearance of new pits, which can form a direct extension to a linear dune gully channel, or form as a "detached" pit. Pits are only ambiguously observed associated with perennial rills, because they are at the limit of the image resolution (Fig. 11).

Because of the very similar timing and association with a surrounding low albedo zone (occasionally observed with a high albedo halo), it seems likely that the processes that form and modify perennial rills are similar to those that trigger the changes observed in active linear dune gullies, yet conditions specific to the Russell Crater megadune cause the perennial rills to express a different morphology. The most notable difference between the Russell Crater megadune and the other sites is its size – it is the largest dune with linear dune gullies on Mars and therefore the linear dune gullies themselves are longer and wider. Hence, any given formation process needs to be able to explain both the peculiar morphology of the perennial rills and that of the linear dune gullies.

Comparison with terrestrial morphologies

The distributary network of channels observed in the perennial rill system is unusual for a mean slope of 12° (Figs. 3, 5d), especially because the topography itself is not convex. In general, a fluvial network on such topography would form a tributary network of contributory channels, or almost-parallel channels, which is also seen for gullies on Mars (Fig.5a). We therefore sought a terrestrial analogue which might inform us about the conditions/processes, which result in a distributary network on such a steep slope angle.

We identified a network of channels on the surface of the glacier Eyjabjakkajökull in Iceland, which share some of their morphological characteristics with the perennial rills on Mars. We made field observations of these channels in July 2009 at the surface of Eyjabjakkajökull, an outlet glacier that drains the north-eastern portion of the Vatnajökull glacier, Iceland (64°39’57’’N, 15°41’54’’W) on glacier slopes ~10°, as measured on the ArcticDEM created by the Polar Geospatial Center from DigitalGlobe, Inc. imagery. Such channels develop in summer in response to surface meltwater flow on temperate glaciers (Fig. 12).

In their proximal sections, the channels are linear, slightly sinuous and run in the direction of steepest slope of the glacier surface. Channel widths reach ~1 m at most and remain almost constant along their ~500 m length (Fig. 12). These channels are thus similar in overall shape and dimensions to the perennial rills observed on the Russell Crater megadune. In their distal sections, these channels split into networks of distributary branches (Fig. 12a), with similar topology to the perennial rills on Mars (Figs. 5d-f). The branching angles are from 45-90° and the individual branches do not necessarily follow the line of greatest slope.

The channels observed at the surface of the Eyjabjakkajökull glacier form during the summer melting period. At this time of the year, the glacier is covered by slush, a mixture of ice crystals and meltwater at the melting point. Meltwater with floating ice particles pours out from springs scattered on the glacier surface, then flows down over the surface of the glacier along channels incised into the slush. In their proximal sections, the channels display little sinuosity and their overall direction follows the steepest slope of the glacier surface. In the channel distal sections, the meltwater infiltrates back into the glacier through a layer of permeable firn. This firn layer is composed of snow accumulated at the glacier surface earlier in the year which has not yet metamorphosed into ice.

The meltwater transports ice particles derived from the surface slush and possibly from the underlying glacier ice. Where the meltwater infiltrates back into the firn, these ice particles accumulate and form a small fan-shaped dam. As this dam builds, meltwater backs up behind the dam, forming a pond. Once this pond reaches a critical size (~1 m in width and ~10 cm in thickness), the meltwater breaks out sideways through the channel wall. The meltwater now flows around the obstacle, forming a new branch that is laterally offset from the previous channel tip. The previous channel tip then becomes inactive.

This damming-ponding-shifting process (Fig. 13) of channel tip propagation repeats again and again through time and eventually leads to the formation of a distributary network (Fig. 12b). The branching pattern in the channel distal sections is thus the result of repeated damming-ponding-shifting events but, at any given time, meltwater flows in only one branch of the network. Some of these channel features described here for Iceland, are also observed in meltwater propagating along gullies in the Antarctic dry valleys (Dickson et al., 2017; Head et al., 2012). The meltwater in the Antarctic dry valleys is produced from snowmelt and thaw of ground ice during peak daytime temperatures and colder temperatures later in the day freeze the meltwater forming a dam. The flow is then reactivated the following day, and deviation around the previous day's frozen deposits causes channel migration. Similarly to Eyjabjakkajökull, the meltwater flows over an impermeable surface (ice table), capped by unsaturated sediment. The Antarctic meltwater flows are surrounded by a halo of saturated ground, forming a dark zone which encircles the flow. A third, yet smaller-scale example of this kind of flow-process is found at the Kobuk sand dunes in Alaska where melting of niveo-aeolian deposits causes small debris flows, with terminal distributary networks on their slip-faces at angles around 16° (Hooper and Dinwiddle 2014). Similarly Hugenholtz et al. (2007) report on morphologies resulting from the melting of niveo-aeolian deposits within dunes at Bigstick Sand Hills of southwestern

Saskatchewan, Canada. Most of the morphologies they report form lobate or digitate deposits with poorly-defined channels, but they did find gully-fan complexes developed in blowout hollows, often cross-cutting the other morphologies, but did not record the slope-angles of this activity.

Cold-room experiments have also shown that channel-formation is favoured when liquid water flows over a thawed surface layer ('active layer') which overlies impermeable permafrost (Jouannic et al., 2015; Conway et al., 2011; Védie et al., 2008). The active layer is composed of non-cohesive material similar to the firn layer in Iceland. During experiments where this layer was dry (Jouannic et al., 2015; Conway et al., 2011), a darker halo of saturated substrate surrounded the channels, similarly to larger meltwater flows in the Antarctic Dry Valleys (Dickson et al., 2017; Head et al., 2012).

Gravity, atmospheric pressure and temperature conditions in these field and laboratory examples are different to those prevailing at the Russell Crater megadune on Mars. Surface materials also probably differ in their composition and physical properties. Therefore, arguing that perennial rills on Mars form by processes identical to those responsible for the development of channels at the surface of Eyjabjakkajökull glacier, for example, would be an over interpretation of their morphological similarities. However, some of the same physical processes may be at work, as discussed further below.

Potential formation mechanisms

Observations from the Icelandic analogue show that a process by which successive blockages and breakouts are created can explain the distributary, branching system exhibited by the perennial rills on Mars. In the Icelandic analogue the conditions which favour development of such a

system are: (i) the presence of an impermeable substrate or a very low infiltration rate, (ii) the presence of a non-cohesive or erodible material at the surface, (iii) a mechanism leading to repeated formation of dams at the front of the flow (high sediment load). The material migrates by this erosional process from the upstream part to the downstream part.

The fact that the perennial rills on Mars diverge from one another argues for the creation of a small amount of relief around the rills, such as lateral levees, even there is no direct observation of this morphology on the images or DTM. This relief, similar to the damming of rills in Iceland, could explain why perennial rills diverge and do not run straight downslope. Some of these deviations could be also influenced by pre-existing aeolian ripples.

On Mars ice cemented permafrost is believed to be present in the first few tens of centimetres to metre of the surface and is overlain with a desiccated layer of regolith (Mellon et al., 2004). This condition is in diffusive equilibrium with the current state of the martian atmosphere and the current daily and seasonal skin depth penetration. Following this logic previous work has shown that at the latitude of the Russell Crater megadune (45°S) the ground ice table should be located at 1 m for sand material (Mellon et al., 2004) and have been estimated to be located at around 1.5 m locally by geomorphologic considerations (Jouannic et al., 2012). It should be noted that on active dunes in the northern hemisphere the ice-cement is inferred to be deep, or absent based on the presence of slip face failures penetrating tens to hundreds of metres into the dune (Diniega et al., 2017; Hansen et al., 2011,2013). On the other hand, Pasquon et al. (2018) argued based on morphology that linear dune gullies should only form in the presence of ground-ice in the near subsurface. This configuration fulfils criteria i) and ii) above. In order to fulfil the final criterion a downslope transport mechanism is required that allows for flow-damming-ponding and release cycles. Below, we discuss the various forms of downslope transport that could be responsible for such rill-systems.

Dry granular flow

The simplest candidate transport mechanism is dry granular flow, which is responsible for slip-face avalanches on terrestrial sand dunes (e.g., Nield et al., 2017; Sutton et al. 2013). However, the rills are found on an average slope of 12° or less and are located at least 200 m away from the crest of the dune which has a slope higher than 25° (Fig. 3). Dry grain flows can only initiate on slopes greater than the static friction angle of sand grains (Allen, 1997). On Earth, the static friction angle of dry granular soils is >~30° (Philipponnat and Hubert, 2000) and on Mars, the Mars Exploration Rovers determined static friction angle for very fine sand as ranging from 30° to 37° (Sullivan et al, 2011). As a consequence, from a physical point of view dry granular flow seems unable to explain the observed initiation angle and the runout distance (350-850 m) of the perennial rills. Second, the rills erode the substrate at these relatively modest slope angles and deviate from straight downhill. The erosive pattern suggests a basal shear stress in excess of that which can be obtained by a dry granular flow on a relatively small slope. For a non-cohesive dry sand of ~200-250 μm on a slope less than 10°, the velocity threshold for erosion is around 0.1-1 ms^{-1} (Gargani, 2004) and would be difficult to reach without any fluid involvement. A granular flow would need to be triggered with an initial velocity to reach this velocity threshold. Third, the relatively high sinuosity and branching angles (Figs. 4 and 5) of perennial rills is not reproduced by experiments or models of dry granular flow (Mangold et al., 2003), however such models do not usually include multiple flows required to reproduce the ponding-damming-cycle.

Wind is the most common trigger for slip face avalanches on Earth, yet wind strength does not significantly influence the angle required to trigger slip face avalanches (Sutton et al. 2013; Pelletier, 2015). Given that the slip-faces of dunes on Mars have been measured to have similar

angles to on Earth (Ewing et al., 2017; Atwood-Stone and McEwen 2013), similarly steep (>30°) slopes should be required to trigger such avalanches on Mars. Slip face avalanches also have a morphology unlike that of perennial rills, they usually possess a broad channel with narrow flanking levees and tongue-shaped deposits (e.g., Sutton et al. 2013; Breton et al. 2008) and whose superposition has not been overserved to develop a distributary network.

Therefore, given these observations, we believe that a fluidised flow is required to explain our observations, as is the case in our Icelandic analogue. Candidate fluidised flows include CO_2-gas supported flows and liquid water/brine supported debris flows, and are discussed further below.

Gas supported flow

Perennial rills grow during the final stages of CO_2 defrosting on the dune, hence CO_2 gas supported flows are an obvious fluid candidate. The presence of dark flows and spots on the image just prior to rill-activity suggests that slab ice is present on the megadune's surface just before their formation. The presence of a high albedo cover at the crest of the dune in the images when the perennial rills first appear, suggests that CO_2 frost may remain, although HiRISE cannot distinguish between H_2O and CO_2 frost (Fig. 4). Furthermore, the hypothesised presence of a water ice-rich permafrost at depth in the Russell Crater megadune should favour the earlier sublimation of CO_2 frost compared to surfaces lacking an ice-rich permafrost (Vincendon et al. 2010; Jouannic. 2012). In the earliest image we have in which the perennial rills first appear, dark flows, dark spots, bright haloes, dust devil tracks and perennial rills all coexist (Fig. 4, MY33). Because of the gradual acceleration in the growth of dark spots and dark flows that we observe, we think that the slab decreases in thickness gradually over time.

643 Pilorget and Forget (2016) hypothesised that viscous debris flow-like morphologies can be
644 produced by gas-supported granular flows beneath the CO_2 ice slab, constrained by an ice-
645 cemented permafrost layer at tens of centimetre depth. The slab is repeatedly lifted and cracked by
646 pressure built up from basal sublimation, similar to the Kieffer model of spider formation (Kieffer
647 et al., 2006). Their modelling used the Russell Crater megadune as their primary case study. The
648 fact that such a flow is confined beneath a lid of CO_2 slab, makes damming-ponding-shifting
649 process less likely, as pressurised flows have less capacity to dam. Pilorget and Forget (2016)'s
650 modelling revealed that activity should be visible from L_s 149° until the sublimation of the slab is
651 complete. This timing is broadly consistent with the first appearance of dark flows (which could
652 be as early as L_s 150° in MY30, and for all MYs L_s 165 Table 1; Fig. 9) and the cyclical breaking
653 could explain the repeated activity of the dark flows as the season progresses. However, it seems
654 to be inconsistent with the timing of the perennial rill activity, which occurs when then CO_2 slab is
655 at its thinnest and restricted to the upper part of the dune (upslope of the perennial rills). Rill-
656 activity could be a result of the final cycle of slab-lifting which ultimately breaks and entrains the
657 slab to create a fluidised flow – a process put forward by Pilorget and Forget (2016). However, if
658 this was the case a spatial relationship might be expected between the dark flows and the rills,
659 which is not observed. Also perennial rills might be expected on every dunefield where the dark
660 flows are observed, which is also not the case.
661 Another hypothesis involving CO_2 is the rapid sublimation of CO_2 ice in the near subsurface
662 producing a density flow analogous to a terrestrial "nuée ardente" (Hoffman, 2002; Cedillo-Flores
663 et al., 2011; Raack et al., 2015). Recent laboratory work has shown that this kind of process could
664 trigger downslope sediment movement of sand-sized particles (Sylvest et. al., 2016, 2018).
665 However, the creation of a fluidised granular flow requires a sustained pore pressure, thus a
666 continuous supply of gas. Pilorget and Forget (2016) suggested such a flow could result from

667 inclusion of sublimating solid CO_2 particles within a granular flow, but this process has not been
668 demonstrated numerically or in the laboratory so there is no morphological information available
669 to compare to the perennial rills. Stewart and Nimmo (2002) suggest CO_2 sublimation in-flow
670 would not evolve sufficient gas to support fluidisation, meaning a sufficient reservoir of CO_2 must
671 initially sublimate to support the flow, but Dundas et al. (2017) argue that the frictional dissipation
672 during flow should be sufficient to sublimate some CO_2 and cause some degree of fluidisation.
673 Whether sufficient CO_2 ice is present at the end of defrosting to fluidise the flows that create the
674 perennial rills remains an open question for future research. .

675 CO_2-gas supported flows are proposed to be analogous in terms of behaviour and final
676 morphology to terrestrial pyroclastic flows (Pilorget and Forget, 2016), which can carve channels
677 and deposit lateral levees and terminal lobate deposits and therefore with multiple flow events
678 could conceivably dam and breach to create distributary networks (e.g. de Haas et al., 2016) . At
679 Ngauruhoe Volcano in New Zealand, distributary "levee and channel" deposits are found on slopes
680 between 10 and 20° (Lube et al. 2007) as a result of pyroclastic density currents, consistent with
681 the morphology expressed by the perennial rills. Further work is required to show that pyroclastic
682 flows are a suitable analogy, considering they are sustained by energies in excess of those generated
683 through sublimation (Conway and Balme, 2016).

684

685 ### *CO_2 blocks*

686 The "slab detachment" model was proposed by Diniega et al (2013), whereby slabs of CO_2 ice
687 detach from the cornice and travel downhill on a cushion of gas expelled by sublimation. The gas
688 expelled from the base of these blocks is able to displace sediment and form depressions in the
689 wake of the block (channels) and when the blocks stop they can form circular pits. CO_2 blocks

690 could conceivably form a distributary network of sinuous channels if many small-sized blocks were
691 released, which were deviated by ripples and the levees left by the passage of previous blocks. This
692 type of propagation could be similar to snowballs or "snow rollers" involved in loose wet
693 avalanches (Fig. 14) where gas is the lubricating fluid rather than liquid water. The reason such
694 small blocks would leave the linear gully channels mid-slope remains unexplained. Work by
695 Mc Keown et al. (2017) has shown that CO_2 blocks can explain the appearance of pits associated
696 with linear dune gully-activity – thus this mechanism can apply to both types of activity. However,
697 pit formation has not unambiguously been identified during the development of perennial rills. The
698 dark zones encompassing both linear dune gully activity (RDF) and also perennial rills could be
699 caused by disturbance of the sediment around the block by the gas being produced as they
700 sublimate. Dundas et al. (2012) reported the presence of a dark halos associated with bright blocks
701 found on the floor of linear dune gully channels on the Russell Crater megadune. It is unclear how
702 the (presumably) smaller blocks creating the perennial rills would create the extensive dark zone
703 surrounding the perennial rills. Further, if the dark zones are caused by disruption of sediments by
704 the CO_2 gas, it is difficult to explain how they persist through the following summer, given that
705 dust devil tracks are erased over a similar period. Further experimental work is needed to better
706 elucidate whether CO_2 blocks can create dark halos and morphologies similar to perennial rill
707 networks.

708 Rill-activity occurs when the last remnants of frost are visible at the crest of the dune and
709 our observations suggest that it may be in the form of slab ice. This is because in the earliest image
710 showing rill-development (MY33, L_s 202°) there dark spots and dark flows are still present, which
711 indicate the presence of slab ice. The new rills appear downslope of the brightest frost deposits
712 hosting the dark flows and spots – the expected configuration if they are formed by blocks
713 separating from the slab. In almost every image immediately following rill-activity (with the

714 exception of MY33) high albedo "spots" are visible (Fig. 4) and these were interpreted by Dundas
715 et al. (2012) as CO_2 ice blocks (because some of them cast shadows) – which would seem to support
716 the CO_2 block hypothesis. However, these blocks do not appear within the perennial rill network,
717 but in the surrounding linear dune gully channels (at bends, termini or tributary junctions) and do
718 not appear to spatially correlate with perennial rills or linear dune gully-activity. On the other hand,
719 presumably the blocks responsible for the perennial rills may be smaller than those associated with
720 the larger linear dune gullies, so may be below the resolution available with HiRISE. Without
721 catching a block "in the act" it is difficult to refute or prove this process is occurring in perennial
722 rills, but this would be a challenging observation to make.
723
724 *Liquid involvement*
725 As demonstrated by the terrestrial analogies a liquid supported debris flow is able to reproduce the
726 morphology of the perennial rills. The dark zone surrounding the perennial rills could be explained
727 by the percolation of water into the pore space, freezing and darkening the albedo as seen in the
728 terrestrial analogues (or removing the fines). The bright halos represent a re-condensed transient
729 surface frost (e.g., Kereszturi et al., 2011a,b). It is, however, difficult to explain the formation of
730 pits associated with active linear dune gullies with liquid water, but recent laboratory simulations
731 have highlighted some unusual morphologies produced by boiling liquid water (Raack et al., 2017;
732 Herny et al. 2018) that could address this issue.
733 The most significant problem comes in explaining the source of this liquid, when water is
734 only transiently metastable on Mars (e.g., Hecht 2002) and latent heat loss is a significant barrier
735 to melting. Recent experimental work has highlighted that even boiling of unstable water can have
736 significant effects on the surface topography (Massé et al., 2016; Raack et al., 2017; Herny et al.

737 2018). Sand can be ejected and accumulated at the front of the flow, which in our scenario could
738 produce an obstacle which deviates the flow, but this was not observed in these experiments (as
739 only individual flows were simulated). As stated at the beginning of this section our current
740 understanding of the martian water cycle indicates that ground ice should be present below the
741 surface of the Russell Crater megadune. Hence, the formation of the perennial rills on the Russell
742 Crater megadune could be periglacial in origin, involving the surface thaw of permafrost and
743 mobilisation of thaw fluids (Costard et al., 2002; Jouannic et al., 2012; Mangold et al., 2003; Védie
744 et al., 2008; Jouannic et al., 2015). Daily average temperatures above 0°C during an extended
745 period are required to thaw the ice in the subsurface because it takes time to propagate the thermal
746 wave to depth in the ground (Costard et al., 2002; Kreslavsky et al., 2008). Using a thermal model
747 of surface and the Thermal Emission Spectrometer (TES) measurements of Russell Crater
748 megadune, Reiss et al. (2010a) calculated the surface temperature between L_s = 200° and L_s = 215°
749 coinciding with the timing of the perennial rill activity. Their results showed that the surface
750 temperatures of the Russell Crater megadune should range from ~195 K to ~275 K (Reiss et al.,
751 2010) and the melting point of water-ice could be reached for a few hours per day in the first few
752 centimetres of the ground. As TES measurements are taken over a ~3x6 km area and insolation
753 models consider only simple surface topography, local temperatures could in fact be higher and
754 last for longer than predicted by Reiss et al. (2010a). Conversely, as the perennial rills are located
755 on a pole-facing slope, local temperatures could also be colder and this is where the last frost is
756 observed (and where it is likely to be thicker).

757 As outlined above, the activity of perennial rills occurs as the last CO_2 ice is finally removed
758 from the surface at ~L_s 200°. At this time the "crocus line" or main boundary of the retreating CO_2
759 seasonal cap has already reached 75°S (Piqueux et al., 2015), meaning the remaining CO_2 ice at
760 the crest of the dune forms a cold trap. This could be a cold trap for water vapour, which is driven

761 out of the regolith in the surrounding terrain as the ambient temperature rises (e.g., Bapst et al.,
762 2015). Removal of CO_2 ice at the surface should locally induce a sudden temperature rise, hence
763 the source of water could be this cold-trapped water vapour in the near-surface regolith. The pulses
764 necessary to create the damming-ponding-breaching morphology (Fig. 13) on the Russell Crater
765 megadune could be generated by the diurnal freeze/thaw cycles of H_2O due to the
766 temperature/humidity variation near the melting point of water in early spring (Reiss et al., 2010a).
767 However, we do not have detailed knowledge of the local humidity conditions during the seasonal
768 cap retreat, and surface frosts observed elsewhere are only microns in thickness (e.g. Svitek and
769 Murray, 1990), so whether the supply from this frost would be sufficient to create hundred-metre
770 landforms is an outstanding problem.
771 In addition, dissolved salts can lower the freezing point and evaporation rates of water (e.g.,
772 Chevrier and Altheide, 2008), hence, further extending the period and duration of melting. The
773 presence of liquid brines on the present martian surface has been already suggested by in-situ
774 observations at the Phoenix landing site (e.g. Chevrier et al., 2009; Renno et al., 2009) and by
775 spectral observations of RSL (Ojha et al., 2015). Renno et al. (2009) also demonstrated, with the
776 investigation of in-situ Phoenix results, that the thermodynamics of freeze-thaw cycles ranging
777 from diurnal to geological time-scales can lead to the formation of saline solutions where ice exists
778 near the surface. From a morphological point of view, the slow melting of brine is able to trigger
779 small channel morphologies (Massé et al., 2016) as observed in perennial rills. However, even
780 though no direct signature of brines has been detected on the rills of the Russell Crater megadune,
781 CRISM data indicate salts could be present at the base of the dune (Fig. 10). This result suggests
782 brines could be formed in the Russell Crater region, but no direct link can be made to the formation
783 of the rills. Brines would only play an important role if water is sourced from the melting of ground
784 ice, because surface frosts would only come into limited contact with the salts.

Although melting of the first few centimetres-decimetres of ground ice could explain the rills, the recharge of this system is an outstanding issue. This problem is somewhat ameliorated by the results of recent experiments (Raack et al., 2017; Herny et al. 2018) which have revealed efficient sediment transport by transient boiling water under martian conditions. These results indicate that less water is required to produce morphologic changes at the surface compared to non-boiling flowing water (which forms the channels in our Icelandic analogue). An average increase in annual insolation over the last 20 kyr in the southern hemisphere of Mars (Laskar et al., 2004) could explain the gradual increase of average surface temperature and, as a consequence, the gradual melting of ground ice at depth. The increasing depth of the melting front with time could be the source of the liquid that is involved in the perennial rill activity. The relatively recent insolation increases could explain why the ground ice has not yet been completely depleted. However, this reservoir is finite and this process will end when the ground ice becomes too deep (1) for ice to melt, or (2) for liquid water to reach the surface. Another option is that because the CO_2 ice forms a cold trap, more water vapour could be emplaced here than usually expected in the martian regolith and this could be the source of fluid for the perennial rills. Further numerical and experimental modelling work are required in order to address the outstanding issues regarding the liquid water/brine hypothesis.

Conclusions

We have described in detail the formation and evolution of perennial rills on the surface of the Russell Crater megadune and discriminate them from the other seasonal processes observed on the dune. These perennial rills recur annually and can grow by up to ~10^4 m^2 per Mars Year in

808 the downslope direction and originate from the channels of linear dune gullies. They comprise a
809 distributary network with high branching angles (~45°) and high sinuosity on slopes of 12° or
810 less. They are surrounded by a larger low albedo zone, which persists through the following
811 summer and can sometimes be seen after the following spring. They appear and grow abruptly in
812 spring between L_s 183° and 221° (likely around L_s 200°) which is when the seasonal CO_2 ice
813 sublimation is coming to end and as the slab-ice is removed, as indicated by the disappearance of
814 dark spots and dark flows and the appearance of dust devil tracks. To our knowledge perennial
815 rills are unique to Russell Crater megadune, but our work suggests that they are produced by a
816 similar process to that which is responsible for annual changes observed in linear dune gullies –
817 hence any proposed formation process needs to explain both sets of observations.
818 Our observations on the formation of similar morphologies on a glacial surface in Iceland,
819 suggests that a distributary network of rills on slopes of 12° or less can be formed by: a) the
820 presence of an impermeable layer at the sub-surface b) an erodible layer on top, and c) the
821 repeated formation of small obstacles at the front of propagating channels. Conditions a) and b)
822 are widely acknowledged to be present on Mars, with an ice-cemented permafrost layer being
823 present under a decimetre to centimetre thick dry lag (Mellon et al., 2004; Jouannic et al., 2012
824 and 2015).
825 We rule-out fully dry flows for perennial rill formation due to the low slope on which they
826 form (>~12°) and their complex topology. We find that sub-slab sublimation generated flows
827 (Pilorget and Forget 2016) are unlikely, because the CO_2 slab is both thin and discontinuous at
828 the time when the perennial rills form. Fluidised granular flows supported by CO_2 gas, analogous
829 to pyroclastic flows on Earth, seem unlikely, because of the energies required to sustain ongoing
830 gas-production in such flows, but further work is needed to verify this for Mars. We find that
831 both levitating CO_2 blocks and liquid water/brine are potential formation mechanisms for

perennial rills (and active linear dune gullies), but both have outstanding difficulties. A lack of analogues or laboratory data means the plausibility of levitating CO_2 blocks producing perennial rill morphologies and the surrounding dark zone is hard to properly assess. However, the timing of the perennial rill activity being coincident with the last phase of defrosting, and the appearance of blocks in the surrounding landscape provides compelling support for this hypothesis. For liquid water/brine hypothesis, the morphologies of the perennial rills are easily accounted for, yet producing liquid water is particularly challenging under current martian conditions. We highlight two factors that could favour the production of liquid water: i) the late-CO_2 forms a cold trap, which could accumulate atmospheric ice, and would then melt upon the sudden temperature rise when the CO_2 is finally removed and ii) increasing mean annual temperatures on Mars could be increasing the depth of the active layer into the shallow ground ice on Russell Crater megadune. However, the formation of pits via water/brine flow is harder to explain, but could be a result of boiling liquid water. Further laboratory work and modelling is required to understand the complex interplay of these volatiles under the rapidly changing springtime conditions on pole-facing slopes of dunefields on Mars in order to better distinguish between these two leading hypotheses.

Acknowledgements

Thank you to the reviewers Colin Dundas and Jan Raack, whose comments helped to improve this paper. This work was supported by “Programme National de Planétologie”, CNRS-INSU. Thanks to the HiRISE team and the Orsay Planetary Picture Library (http://fototek.geol.u-psud.fr), as well as the HRSC Team for the data provided. SJC is supported by the French Space

855 Agency CNES for her HiRISE related work. The ArcticDEM used in this work was created by
856 the Polar Geospatial Center from DigitalGlobe, Inc. imagery, DEMs provided under NSF OPP
857 awards 1043681, 1559691 and 1542736.

References

Achilles, C. N. et al (2017), Mineralogy of an Active Eolian Sediment from the Namib Dune, Gale Crater, Mars, J. Geophys. Res. Planets, 122, doi:10.1002/2017JE005262.

Allen, P.A., 1997. Earth Surface Processes. Blackwell Science, Oxford.

Atwood-Stone, C., McEwen, A.S., 2013. Avalanche slope angles in low-gravity environments from active Martian sand dunes. Geophysical Research Letters 40, 2929–2934. doi:10.1002/grl.50586

Auld, K.S., Dixon J.C., 2016. A classification of martian gullies from HiRISE imagery. Planetary and Space Science 131, 88-101.

Balme, M., Greeley, R., 2006. Dust devils on Earth and Mars. Rev. Geophys. 44, RG3003, doi:10.1029/2005RG000188.

Balme, M., Mangold, N., Baratoux, D., Costard, F., Gosselin, M., Masson, P., Pinet, P., Neukum, G., 2006. Orientation and distribution of recent gullies in the southern hemisphere of Mars: Observations from High Resolution Stereo Camera/Mars Express (HRSC/MEX) and Mars Orbiter Camera/Mars Global Surveyor (MOC/MGS) data. J. Geophys. Res. 111, E05001, doi:10.1029/2005JE002607.

881 Bapst, J., Bandfield, J.L., Wood, S.E., 2015. Hemispheric asymmetry in martian seasonal surface
882 water ice from MGS TES. Icarus 260, 396–408. doi:10.1016/j.icarus.2015.07.025
883
884 Breton, C., Lancaster, N., Nickling, W.G., 2008. Magnitude and frequency of grain flows on a
885 desert sand dune. Geomorphology 95, 518–523. doi:10.1016/j.geomorph.2007.07.004
886
887 Brown, A.J., Calvin, W.M., McGuire, P.C., Murchie, S.L., 2010. Compact Reconnaissance
888 Imaging Spectrometer for Mars (CRISM) south polar mapping: First Mars Year of observations.
889 J. Geophys. Res. 115, E00D13. Doi: 10.1029/2009JE003333.
890
891 Cantor, B.A., Kanak, K.M., Edgett, K.S., 2006. Mars Orbiter Camera observations of Martian
892 dust devils and their tracks (September 1997 to January 2006) and evaluation of theoretical
893 vortex models. J. Geophys. Res. 111, E12002. doi:10.1029/2006JE002700.
894
895 Carter, J., Poulet, F., Murchie, S., Bibring, J.-P., 2013. Automated processing of planetary
896 hyperspectral datasets for the extraction of weak mineral signatures and applications to CRISM
897 observations of hydrated silicates on Mars. Planetary and Space Science 76, 53-67,
898 doi:10.1016/j.pss.2012.11.007.
899
900 Ceamanos, X., Douté, S., Luo, B., Schmidt, F., Jouannic, G.; Chanussot, J., 2011.
901 Intercomparison and validation of techniques for spectral unmixing of hyperspectral images: a
902 planetary case study. IEEE Transactions on Geoscience and Remote Sensing,
903 doi:10.1109/TGRS.2011.2140377.

Cedillo-Flores, Y., Treiman, A.H., Lasue, J., Clifford, S.M., 2011. CO_2 fluidization in the initiation and formation of Martian polar gullies. Geophys. Res. Lett. 38, L21202, doi:10.1029/2011GL049403.

Chevrier, V.F., Ulrich, R., Altheide, T.S., 2009. Viscosity of liquid ferric sulfate solutions and application to the formation of gullies on Mars. J. Geophys. Res. 114, E06001, doi:10.1029/2009JE003376.

Chevrier, V.F., Altheide, T.S., 2008. Low temperature aqueous ferric sulfate solutions on the surface of Mars. Geophys. Res. Lett. 35, L22101, doi: 10.1029/2008GL035489.

Christensen, P.R., Kieffer, H.H., Titus, T.N., 2005. Infrared and visible observations of south polar spots and fans. American Geophysical Union, Fall Meeting Abstract P23C-04.

Conway, S.J., Lamb, M.P., Balme, M.R., Towner, M.C., Murray, J.B., 2011. Enhanced runout and erosion by overland flow at low pressure and sub-freezing conditions: Experiments and application to Mars. Icarus 211, 443-457, doi:10.1016/j.icarus.2010.08.026.

Conway, S.J., Balme, M.R., 2016. A novel topographic parameterization scheme indicates that martian gullies display the signature of liquid water. Earth and Planetary Science Letters 454, 36–45. https://doi.org/10.1016/j.epsl.2016.08.031

Conway, S.J., Harrison, T.N., Soare, R.J., Britton, A.W. & Steele, L.J. 2017. New slope-normalized global gully density and orientation maps for Mars. In: Conway, S.J., Carrivick, J.L., Carling, P.A., de Haas, T. & Harrison, T.N. (eds) Martian Gullies and their Earth Analogues. Geological Society, London, Special Publications, 467. First published online November 27, 2017, https://doi.org/10.1144/SP467.3

Conway, S., de Haas, T. & Harrison, T.N. 2018. Martian gullies: a comprehensive review of observations, mechanisms and the insights from Earth analogues. In: Conway, S.J., Carrivick, J.L., Carling, P.A., de Haas, T. & Harrison, T.N. (eds) Martian Gullies and their Earth Analogues. Geological Society, London, Special Publications, 467. First published online [to follow] (17-313), https://doi.org/10.1144/SP467.14

Costard, F., Forget, F., Mangold, N., Peulvast, J.P., 2002. Formation of recent Martian debris flows by melting of near-surface ground ice at high obliquity. Science 295, 110-113, doi: 10.1126/science.295.5552.110.

Cull, S., Arvidson, R. E., Mellon, M., Wiseman, S., Clark, R., Titus, T., Morris, R. V., McGuire, P., 2010. Seasonal H2O and CO2 ice cycles at the Mars Phoenix landing site: 1. Prelanding CRISM and HiRISE observations. J. Geophys. Res. 115, doi:10.1029/2009JE003340.

de Haas, T., van den Berg, W., Braat, L., Kleinhans, M.G., 2016. Autogenic avulsion, channelization and backfilling dynamics of debris-flow fans. Sedimentology 63, 1596–1619. doi:10.1111/sed.12275

951 Dickson, J.L., Head, J.W., Levy, J.S., Morgan, G.A. & Marchant, D.R. 2017. Gully formation in
952 the McMurdo Dry Valleys, Antarctica: multiple sources of water, temporal sequence and relative
953 importance in gully erosion and deposition processes. In: Conway, S.J., Carrivick, J.L., Carling,
954 P.A., de Haas, T. & Harrison, T.N. (eds) Martian Gullies and their Earth Analogues. Geological
955 Society, London, Special Publications, 467. First published online December 4, 2017,
956 https://doi.org/10.1144/SP467.4
957
958 Diniega, S., 2014. Linear Gullies (Mars), in: Hargitai, H., Kereszturi, Á. (Eds.), Encyclopedia of
959 Planetary Landforms. Springer New York, New York, NY, pp. 1–5. doi:10.1007/978-1-4614-
960 9213-9_582-1
961
962 Diniega, S., Byrne, S., Bridges, N.T., Dundas, C.M., McEwen, A.S., 2010. Seasonality of
963 present-day Martian dune-gully activity. Geology 38, 1047-1050, doi: 10.1130/G31287.1.
964
965 Diniega, S., Hansen, C.J., McElwaine, J.N., Hugenholtz, C.H., Dundas, C.M., McEwen, A.S.,
966 Bourke, M.C., 2013. A new dry hypothesis for the formation of martian linear gullies. Icarus 225,
967 526–537. doi:10.1016/j.icarus.2013.04.006
968
969 Diniega, S., Hansen, C.J., Allen, A., Grigsby, N., Li, Z., Perez, T. & Chojnacki, M. 2017. Dune-
970 slope activity due to frost and wind throughout the north polar erg, Mars. In: Conway, S.J.,
971 Carrivick, J.L., Carling, P.A., de Haas, T. & Harrison, T.N. (eds) Martian Gullies and their Earth
972 Analogues. Geological Society, London, Special Publications, 467. First published online
973 November 27, 2017, https://doi.org/10.1144/SP467.6
974

Dundas, C.M., McEwen, A.S., Diniega, S., Byrne, S., Martinez-Alonso, S., 2010. New and recent gully activity on Mars as sees by HiRISE. Geophys. Res. Lett. 37, L07202, doi: 10.1029/2009GL041351

Dundas, C.M., Diniega, S., Hansen, C.J., Byrne, S., McEwen, A.S., 2012. Seasonal activity and morphological changes in Martian gullies. Icarus 220, 124-143, doi:10.1016/j.icarus.2012.04.005

Dundas, C.M., Diniega, S., McEwen, A.S., 2015. Long-term monitoring of martian gully formation and evolution with MRO/HiRISE. Icarus 251, 244–263 http: //dx.doi.org/10.1016/j.icarus.2014.05.013

Dundas, C.M., McEwen, A.S., Diniega, S., Hansen, C.J., Byrne, S. & McElwaine, J.N. 2017. The formation of gullies on Mars today. In: Conway, S.J., Carrivick, J.L., Carling, P.A., de Haas, T. & Harrison, T.N. (eds) Martian Gullies and their Earth Analogues. Geological Society, London, Special Publications, 467. First published online November 27, 2017, https://doi.org/10.1144/SP467.5

Ewing, R. C. et al 2017. Sedimentary processes of the Bagnold Dunes: Implications for the eolian rock record of Mars, J. Geophys. Res. Planets, 122, doi:10.1002/2017JE005324.

Fisher, J.A., Richardson, M.I., Newman, C.E., Szwast, M.A., Graf, C., Basu, S., Ewald, S.P., Toigo, A.D., Wilson, R.J., 2005. A survey of Martian dust devil activity using Mars Global

998 Surveyor Mars Orbiter Camera images. J. Geophys. Res. 110, E03004.
999 doi:10.1029/2003JE002165.
1000
1001 Gardin, E., Allemand, P., Quantin, C., Thollot,, P. , 2010. Defrosting, dark flow features and
1002 dune activity on Mars: example in Russell Crater. J. Geophys. Res. 115, E06016,
1003 doi:10.1029/2009JE003515.
1004
1005 Gargani, J., 2004. Contribution à l'étude de la vitesse critique d'érosion des sols cohésifs, C.R.
1006 Geoscience, 336, p.561-566, 2004.
1007
1008 Gough, R.V., Chevrier, V.F., Baustian, K.J., Wise, M.E., Tolbert, M.A., 2011. Laboratory studies
1009 of perchlorate phase transitions: Support for metastable aqueous perchlorate solutions on Mars.
1010 Earth Planet. Sci. Lett. 312, 371-377, doi:10.1016/j.epsl.2011.10.026.
1011 Gwinner, K., Scholten, F. et al. 2009. Derivation and validation of high-resolution digital
1012 elevation models from Mars Express HRSC-data. Photogrammetric Engineering & Remote
1013 Sensing, 75, 1127– 1142.
1014
1015 Greeley, R., 2005. Martian variable features: New insight from the Mars Express Orbiter and the
1016 Mars Exploration Rover Spirit. Journal of Geophysical Research 110.
1017 https://doi.org/10.1029/2005JE002403
1018
1019 Hanley, J., V. F. Chevrier, J. B. Dalton, and C. S. Jamieson, 2011, Reflectance spectra of low-
1020 temperature chloride and perchlorate hydrates relevant to planetary remote sensing. 42nd Lunar
1021 and Planetary Science Conference, abstract# 2327.

Hansen, C.J., Thomas, N., Portyankina, G., McEwen, A., Becker, T., Byrne, S., Herkenhoff, K., Kieffer, H., Mellon, M., 2010. HiRISE observations of gas sublimation-driven activity in Mars' southern polar regions: I. Erosion of the surface. Icarus 205, 283–295. https://doi.org/10.1016/j.icarus.2009.07.021

Hansen, C.J., Bourke, M., Bridges, N.T., Byrne, S., Colon, C., Diniega, S., Dundas, C., Herkenhoff, K., McEwen, A., Mellon, M., Portyankina, G., Thomas, N., 2011. Seasonal Erosion and Restoration of Mars's Northern Polar Dunes. Science 331, 575-578, doi: 10.1126/science.1197636.

Hansen, C.J., Byrne, S., Portyankina, G., Bourke, M., Dundas, C., McEwen, A., Mellon, M., Pommerol, A., Thomas, N., 2013. Observations of the northern seasonal polar cap on Mars: I. Spring sublimation activity and processes. Icarus 225, 881–897. https://doi.org/10.1016/j.icarus.2012.09.024

Head, J., Dickson, J. L., Levy, J. S., Baker, D. M. H., Marchant, D. R., 2012. Antarctic Dry Valleys: Geological Processes in Hyperarid, Hypothermal Environments and Implications for Water on Mars. Geophysical Research Abstracts 14, EGU2012-12381-1.

Hecht, M.H., 2002. Metastability of liquid water on Mars. Icarus 156, 373–386. doi:10.1006/icar.2001.6794

Herny, C., Conway, S.J., Raack, J., Carpy, S., Colleu-Banse, T. & Patel, M.R. 2018. Downslope sediment transport by boiling liquid water under Mars-like conditions: experiments and potential implications for Martian gullies. In: Conway, S.J., Carrivick, J.L., Carling, P.A., de Haas, T. & Harrison, T.N. (eds) Martian Gullies and their Earth Analogues. Geological Society, London, Special Publications, 467. First published online February 6, 2018, https://doi.org/10.1144/SP467.10

Hoffman, N., 2002. Active polar gullies on Mars and the role of carbon dioxide. Astrobiology 2, 313-323, doi:10.1089/153110702762027899.

Hooper, D.M., Dinwiddie, C.L., 2014. Debris flows on the Great Kobuk Sand Dunes, Alaska: Implications for analogous processes on Mars. Icarus 230, 15–28. doi:10.1016/j.icarus.2013.07.006

Hugenholtz, C.H., Wolfe, S.A., Moorman, B.J., 2007. Sand–water flows on cold-climate eolian dunes: environmental analogs for the eolian rock record and Martian sand dunes. Journal of Sedimentary Research 77, 607–614. Doi: 10.2110/jsr.2007.063

Ivanov, A. B., Muhleman, D. O., 2001. Cloud Reflection Observations: Results from the Mars Orbiter Laser Altimeter. Icarus 154 (1), 190-206.

Jouannic, G., Gargani, J., Costard, F., Ori, G.G., Marmo, C., Schmidt, F., Lucas, A., 2012. Morphological and mechanical characterization of gullies in a periglacial environment: the case of the Russell dune (Mars). Planetary and Space Science 71, 38-54, doi:10.1016/j.pss.2012.07.005.

Jouannic, G. 2012. PhD Thesis. Geomorphologic study of the dynamic of debris flow formation on Mars : comparative approach Earth / Mars. University Paris-Sud, 264 p.

Jouannic G., J.Gargani, S. Conway, F. Costard, M. Balme, M. Patel, M. Massé, C. Marmo, V. Jomelli, G. Ori. 2015. Laboratory simulation of debris flows over a sand dune: Insights into gully-formation (Mars). Geomorphology, 231, 101-115.

Kereszturi, A., Möhlmann, D., Berczi, Sz., Ganti, T., Kuti, A., Sik, A., Horvath, A., 2009. Recent rheologic processes on dark polar dunes of Mars: Driven by interfacial water? Icarus 201, 492-503, doi: 10.1016/j.icarus.2009.01.014.

Kereszturi, A., Möhlmann, D., Berczi, S., Ganti, T., Horvath, A., Kuti, A., Sik, A., Szathmary, E., 2010. Indications of brines related local seepage phenomena on the northern hemisphere of Mars. Icarus 207, 149-164, doi: 10.1016/j.icarus.2009.10.012.

Kereszturi, A., Vincendon, M., Schmidt, F., 2011a. Water ice in the dark dune spots of Richardson crater on Mars. Planetary and Space Science 59, 26-42, doi: 10.1016/j.pss.2010.10.015.

Kereszturi, A., Möhlmann, D., Berczi, S., Ganti, T., Horvath, A., Sik, A., Szathmary, E., 2011b. Possible role of brines in the darkening and flow-like features on the Martian polar based on HiRISE images. Planetary and Space Science 59, 1413-1427, doi: 10.1016/j.pss.2011.05.012.

Kieffer, H.H., Christensen, P.R., Titus, T.N., 2006. CO_2 jets formed by sublimation beneath translucent slab ice in Mars' seasonal south polar ice cap. Nature 442, 793–796, doi: 10.1038/nature04945.

Kieffer, H. H., 2007. Cold jets in the Martian polar caps. J. Geophys. Res., 112, E08005, doi:10.1029/2006JE002816.

Kirk, R.L., Howington-Kraus, E., Rosiek, M.R., Anderson, J.A., Archinal, B.A., Becker, K.J., Cook, D.A. et al., 2008. Ultrahigh resolution topographic mapping of Mars with MRO HiRISE stereo images: Meter-scale slopes of candidate Phoenix landing sites. J. Geophys. Res., 113, doi:10.1029/2007JE003000.

Kossacki, J.K., Kopystynski, L., 2004. Non-uniform seasonal defrosting of subpolar dune filed on Mars. Icarus 168, 201–204, doi: 10.1016/j.icarus.2003.11.010.

Kreslavsky, M.A., Head, J.W., Marchant, D.R., 2008. Periods of active permafrost layer formation during the geological history of Mars: Implications for circum-polar and mid-latitude surface processes. Planet. Space Sci. 56, 289-302, doi: 10.1016/j.pss.2006.02.010.

Laskar, J., Correia, A.C.M., Gastineau, M., Joutel, F., Levrard, B., Robutel, P., 2004. Long term evolution and chaotic diffusion of the insolation quantities of Mars. Icarus 170, 343-364, doi:10.1016/j.icarus.2004.04.005.

Lube, G., Cronin, S.J., Platz, T., Freundt, A., Procter, J.N., Henderson, C., Sheridan, M.F., 2007. Flow and deposition of pyroclastic granular flows: A type example from the 1975 Ngauruhoe

eruption, New Zealand. Journal of Volcanology and Geothermal Research 161, 165–186. doi:10.1016/j.jvolgeores.2006.12.003

Malin, M.C. and 15 colleagues, 1998. Early views of the Martian surface from the Mars orbiter camera of Mars Global Surveyor. Science 279, 1681–1685, doi: 10.1126/science.279.5357.1681.

Malin, M.C., Edgett, K.S., 2001. Mars Global Surveyor Mars Orbiter Camera: Interplanetary cruise through primary mission. J. Geophys. Res. 106, 23429-3570, doi: 10.1029/2000JE001455.

Mangold, N., Costard, F., Forget, F., 2003. Debris flows over sand dunes on Mars: Evidence for liquid water. J. Geophys. Res. 108, 5027, doi:10.1029/2002JE001958.

Massé M., Conway S., Gargani J., M. R. Patel, K. Pasquon, A. McEwen, S. Carpy, V. Chevrier, M. R. Balme, L. Ojha, M. Vincendon, F. Poulet, F. Costard, G. Jouannic, 2016. Transport processes induced by metastable boiling water under Martian surface conditions. Nature Geoscience, 9, 425-428.

Mellon, M.T., Feldman, W.C., Prettyman, T.H., 2004. The presence and stability of ground ice in the southern hemisphere of Mars. Icarus 169, 324–340.

Möhlmann, D., 2010. Temporary liquid water in upper snow/ice sub-surfaces on Mars? Icarus 207, 140-148, doi: 10.1016/j.icarus.2009.11.013.

Möhlmann, D., 2011. Latitudinal distribution of temporary liquid cryobrines on Mars. Icarus 214, 236-239, doi: 10.1016/j.icarus.2011.05.006.

1145 Möhlmann, D., Thomsen, K., 2011. Properties of cryobrines on Mars. Icarus 212, 123-130, doi:
1146 10.1016/j.icarus.2010.11.025.
1147
1148 Neakrase, L.D.V., Balme, M.R., Esposito, F. et al. , 2016 Space Sci Rev. 203: 347.
1149 doi:10.1007/s11214-016-0296-6
1150
1151 Nield, J. M., Wiggs, G. F., Baddock, M. C., & Hipondoka, M. H., 2017. Coupling leeside
1152 grainfall to avalanche characteristics in aeolian dune dynamics. Geology, 45(3), 271-274, doi:
1153 10.1130/G38800.1
1154
1155 Ojha, L., Wilhelm, M.B., Murchie, S.L., McEwen A.S., Wray J.J., Hanley J., Massé
1156 M., Chojnacki M., 2015. Spectral evidence for hydrated salts in seasonal flows on Mars. Nature
1157 Geoscience, 8, 829-832. doi:10. 1038/ngeo2546
1158
1159 Pasquon, K., Gargani, J., Massé, M., Conway, S.J., 2016. Present day formation and seasonal
1160 evolution of linear dune gullies on Mars. Icarus 274, 195-210.
1161
1162 Pasquon K., J. Gargani, M. Nachon, M. Massé, S. J. Conway, G. Jouannic, M.Balme, F. Costard,
1163 M. Vincendon, 2018. Are the different gully morphologies due to different processes on the
1164 Kaiser dune field? in: Conway S.J., Carrivick J. L., Carling P. A., de Haas T. and Harrison T. N.
1165 (Eds.), Martian Gullies and their Earth Analogues. The Geological Society of London, Special
1166 Publications, 467, https://doi-org.insu.bib.cnrs.fr/10.1144/SP467.13
1167

Pelletier, J.D., 2015. Controls on the large-scale spatial variations of dune field properties in the barchanoid portion of White Sands dune field, New Mexico: Controls on dunes at White Sands. Journal of Geophysical Research: Earth Surface 120, 453–473. https://doi.org/10.1002/2014JF003314

Philipponnat, G., Hubert, B., 2000. Fondations et ouvrages en Terre, second edition Eyrolles Edition, France.

Pilorget, C., Forget, F., 2016. Formation of gullies on Mars by debris flows triggered by CO2 sublimation. Nature Geosci 9, 65–69. https://doi.org/10.1038/ngeo2619

Piqueux, S., Byrne, S., Richardson, M.I., 2003. Sublimation of Mars' southern seasonal CO_2 ice cap and the formation of spiders, J. Geophys. Res. 108, E85084, doi:10.1029/2002JE002007.

Piqueux, S., Kleinböhl, A., Hayne, P.O., Kass, D.M., Schofield, J.T., McCleese, D.J., 2015. Variability of the martian seasonal CO_2 cap extent over eight Mars Years. Icarus 251, 164–180. doi:10.1016/j.icarus.2014.10.045

Raack, J., Conway, S.J., Herny, C., Balme, M.R., Carpy, S., Patel, M.R., 2017. Water induced sediment levitation enhances down-slope transport on Mars. Nature Communications 8, 1151. https://doi.org/10.1038/s41467-017-01213-z

1190 Raack, J., Reiss, D., Appéré, T., Vincendon, M., Ruesch, O., Hiesinger, H., 2015. Present-Day
1191 Seasonal Gully Activity in a South Polar Pit (Sisyphi Cavi) on Mars. Icarus 251, 226–243.
1192 https://doi.org/j.icarus.2014.03.040
1193
1194 Reiss, D., Erkeling, G., Bauch, K.E., Hiesinger, H., 2010a. Evidence for present day gully
1195 activity on the Russell crater dune field, Mars. Geophys. Res. Lett. 37, L06203,
1196 doi:10.1029/2009GL042192.
1197
1198 Reiss, D., Raack, J., Rossi, A.P., Di Achille, G., Hiesinger, H., 2010b. First in-situ analysis of
1199 dust devil tracks on Earth and their comparison with tracks on Mars. Geophysical Research
1200 Letters 37, n/a-n/a. https://doi.org/10.1029/2010GL044016
1201
1202 Reiss. D., Zanetti, M., Neukum, G., 2011a. Multitemporal observations of identical active dust
1203 devils on Mars with the High Resolution Stereo Camera (HRSC) and Mars Orbiter Camera
1204 (MOC). Icarus 215, 358-369, doi:10.1016/j.icarus.2011.06.011.
1205
1206 Reiss, D., Raack, J., Hiesinger, H., 2011b. Bright dust devil tracks on Earth: Implications for their
1207 formation on Mars. Icarus 211, 917–920. https://doi.org/10.1016/j.icarus.2010.09.009
1208
1209 Reiss, D., and R. Jaumann, 2003. Recent debris flows on Mars: Seasonal observations of the
1210 Russell Crater dune field, Geophys. Res. Lett., 30, 1321, doi:10.1029/2002GL016704, 6.
1211
1212 Renno, N.O., Bos, B. J., Catling, D., Clark, B.C., Drube, L., Fisher, D., Goetz, W., Hviid, S. F.,
1213 Keller, H. U., Kok, J. F., Kounaves, S. P., Leer, K., Lemmon, M., Madsen, M. B., Markiewicz,

W. J., Marshall, J., McKay, C., Mehta, M., Smith, M., Zorzano, M. P., Smith, P. H., Stoker, M., Young, S. M., 2009. Possible physical and thermodynamical evidence for liquid water on Mars. J. Geophys. Res. 114, E00E03, doi:10.1029/2009JE003362.

Scholten, F., Gwinner, K., Roatsch, T., Matz, K.-D., Wählisch, B., Giese, B., Oberst, J., Jaumann, R., Neukum, G., 2005. Mars Express HRSC Data Processing – Methods and Operational Aspects. Photogramm. Eng. Remote Sens. 71, 1143–1152.

Smith, D. E., Zuber, M. T., Neumann, G. A., 2001. Seasonal Variations of Snow Depth on Mars. Science 294 (5549), 2141-2146.

Stanzel, C., Pätzold, M., Greeley, R., Hauber, E., Neukum, G., 2006. Dust devils on Mars observed by the High Resolution Stereo Camera. Geophys. Res. Lett. 33, L11202. doi:10.1029/2006GL025816.

Stewart, S.T., Nimmo, F., 2002. Surface runoff features on Mars: Testing the carbon dioxide formation hypothesis. J. Geophys. Res.-Planets 107, doi:10.1029/2000JE001465.

Sullivan, R., Anderson, R., Biesiadecki, J., Bond, T., Steward, H., 2011. Cohesions, friction angles, and other physical properties of Martian regolith from Mars Exploration Rover wheel trenches and wheel scuffs. J. Geophys. Res. 116, E02006, doi:10.1029/2010JE003625.

Sutton, S.L.F., McKenna Neuman, C., Nickling, W., 2013. Lee slope sediment processes leading to avalanche initiation on an aeolian dune. Journal of Geophysical Research: Earth Surface 118, 1754–1766. doi:10.1002/jgrf.20131

Svitek, T., Murray, B., 1990. Winter frost at Viking Lander 2 site. Journal of Geophysical Research 95, 1495. https://doi.org/10.1029/JB095iB02p01495

Sylvest, M.E., Conway, S.J., Patel, M.R., Dixon, J.C., Barnes, A., 2016. Mass wasting triggered by seasonal CO_2 sublimation under Martian atmospheric conditions: Laboratory experiments. Geophysical Research Letters 43, 12,363–12,370. doi:10.1002/2016GL071022

Sylvest, M.E., Dixon, J.C., Conway, S.J., Patel, M.R., McElwaine, J.N., Hagermann, A. & Barnes, A. 2018. CO2 sublimation in Martian gullies: laboratory experiments at varied slope angle and regolith grain sizes. In: Conway, S.J., Carrivick, J.L., Carling, P.A., de Haas, T. & Harrison, T.N. (eds) Martian Gullies and their Earth Analogues. Geological Society, London, Special Publications, 467. First published online February 26, 2018, https://doi.org/10.1144/SP467.11

Thomas, P., Gierasch, P.J., 1985. Dust devils on Mars. Science 230, 175-177, doi: 10.1126/science.230.4722.175.

Thomas, N., Hansen, C.J., Portyankina, G., Russell, P.S., 2010. HiRISE observations of gas sublimation-driven activity in Mars' southern polar regions: II. Surficial deposits and their origins. Icarus 205, 296–310. https://doi.org/10.1016/j.icarus.2009.05.030

Tirsch, D., Jaumann, R., Pacifici, A., Poulet, F., 2011. Dark Aeolian sediments in Martian craters: Composition and sources. J. Geophys. Res. 116, E03002, doi:10.1029/2009JE003562.

Turcotte, D.L., 1997. Fractals and Chaos in Geology and Geophysics, Cambridge University Press, Cambridge.

Védie, E., Costard, F., Font, M., Lagarde, J.L., 2008. Laboratory simulations of Martians gullies on sand dunes. Geophys. Res. Lett. 35, L21501, doi:10.1029/2008GL035638.

Verba, C.A., Geissler, P.E., Titus, T.N., Waller, D., 2010. Observations from the High Resolution Imaging Science Experiment (HiRISE): Martian dust devils in Gusev and Russell craters. J. Geophys. Res. 115, E09002, doi:10.1029/2009JE003498.

Vincendon, M., Mustard, J., Forget, F., Kreslavsky, M., Spiga, A., Murchie, S., Bibring, J.-P., 2010. Near-tropical subsurface ice on Mars. Geophysical Research Letters 37, doi:10.1029/2009GL041426. doi:10.1029/2009gl041426

Figure Captions

Figure 1. Location of the Russell Crater megadune. (**a**) Colour-coded Mars Orbiter Laser Altimeter (MOLA) elevation data with overlain THEMIS Day IR Controlled Mosaic from USGS Astrogeology centred on Russell Crater, with inset bottom-left showing its location on the global MOLA hillshade map. The location of panel (b) is marked with a black box. (**b**) The THEMIS Day IR Controlled Mosaic overlain with CTX (ConTeXt camera) image F06_038335_1253 showing the location of the studied megadune within the Russell crater dunefield and of Figure 3 in the black box. North is up in all images. MOLA credit: NASA/JPL/MOLA Science team. CTX image credit: NASA/JPL-Caltech/MSSS.

Figure 2. Summary of the presently active (perennial and ephemeral) processes observed at the surface of the Russell Crater megadune. (**a**) Perennial rills (HiRISE image ESP_021918_1255, L_s = 265°). (**b**) Dark flows (HiRISE image PSP_002548_1255; L_s = 182°); c) Dark spots (HiRISE image PSP_002548_1255; L_s = 182°). (**d**) Bright halos (HiRISE image ESP_020784_1255, L_s = 210°). (**e**) Dust devil tracks (HiRISE image PSP_005383_1255, L_s = 323°). HiRISE Image credits: NASA/JPL/University of Arizona. North is up in all images.

Figure 3. Overview of perennial rills within the study site. (**a**) Location map of the perennial rills on the Russell Crater megadune, CTX image F06_038335_1253 overlain with HiRISE image PSP_003326_1255 labelled with numbered Zones referred to in the text. (**b**) CTX image overlain with slope map derived from a 10 m/pix median filter smoothed HiRISE digital elevation model DTEEC_007018_1255_007229_1255_A01. The colours are explained in the key. The topographic profile line A-A’ was located along the line of steepest decent (perpendicular to

contour lines). (**c**) Topographic long profile A-A'whose position is shown in panel (b). Slopes indicated for each segment are calculated using a linear least squares fit over all the elevation points in each segment. HiRISE Image credit: NASA/JPL/University of Arizona. CTX image credit: NASA/JPL-Caltech/MSSS.

Figure 4. Evolution of the perennial rill system in Zone 1 of the Russell Crater megadune over 6 Mars Years with each image taken in early spring. The surface area of the perennial rills increases each Mars Year, the extent from the previous year is indicated with a dotted yellow outline. Image numbers are: (**a**) PSP_003326_1255, (**b**) ESP_012213_1255, (**c**) ESP_020784_1255, (**d**) ESP_029764_1255, (**e**) ESP_038335_1255, and (**f**) ESP_047078_1255. HiRISE Image credits: NASA/JPL/University of Arizona.

Figure 5. Evolution of the distal reaches of the perennial rills. (**a-f**) Changes in rill morphology inside a linear dune gully are visible between HiRISE images PSP_003326_1255, ESP_012213_1255, and ESP_020784_1255. (**a**) In MY 28 (L_s = 217.8°), a small rill has lengthened by ~86 m (arrowed and marked by an appearance of low albedo zone) within a wider pre-existing gully-channel and the dark zone has grown by ~16600 m^2. (**b**) In the next Mars Year (MY 29, L_s = 221.2°), the dark zone has further expanded by ~10000 m^2 and the rill lengthened by ~145 m (marked by arrows). (**c**) By MY 30 (L_s = 209.9°) the dark zone has expanded by a further ~9300 m^2 and the rill lengthened by ~190 m. Panels (**d**), (**e**) and (**f**) are detailed cutouts from parts (a), (b) and (c) focussing on the distal part of perennial rills and highlighting the digitate pattern of secondary rills downslope of the major rills. Panels (**g**) and (**h**) show the partial disappearance of small secondary rills (white arrows) located around the central major rill in HiRISE images PSP_003326_1255 and PSP_012213_1255, which may be due to deposition of

aeolian material between the two images (the surface develops ripples). (**i**) Appearance of small new rills in ESP_020784_1255 (grey arrows), where 3 new small branches appear at the terminus of the major rill. HiRISE Image credits: NASA/JPL/University of Arizona. North is up in all images.

Figure 6. Evolution of the upstream part of the perennial rill over 3 Mars Years (MY 28-30). The black continuous lines in panels b1-b3 correspond to the major rills that remain unchanged from one Mars Year to the next. The black dashed lines in panels b1-b3 correspond to rills that are disappearing (probably becoming infilled). The white continuous lines in panels b1-b3 correspond to new major rills formed in the preceding Mars Year. There are few changes in this part of the network, compared to downstream (compare with Fig. 5). HiRISE Image credits: NASA/JPL/University of Arizona. North is up in all images.

Figure 7. The evolution in fractal dimension of the perennial rills in Zone 1 over MY 28-32 (the dark zone in MY33 was only partly visible, so the new parts of the network could not be easily ascertained). (**a**) The evolution of the rill network in Zone 1 represented by linework in MY 28-32 (shown as images in Fig. 4). (**b**) Log-log plot of number of grid-squares containing rills (N) against the grid-spacing (r). The gradient of the linear regression line gives an estimate of the fractal dimension (D) of the perennial rills for each Mars Year, and is indicated in the legend.

Figure 8. Series of HiRISE images showing the seasonal evolution of (**a**) dust devil tracks, (**b**) dark flows, (**c**) dark spots and (**d**) bright halos on Russell Crater megadune. a1) PSP_002548_1255; a2) PSP_003326_1255; a3) PSP_004038_1255; a4) PSP_005383_1255; a5) PSP_005528_1255; a6) PSP_007018_1255; b1) ESP_001440_1255; b2) PSP_001981_1255; b3)

PSP_002337_1255; b4) PSP_002548_1255; b5) PSP_002904_1255; b6) PSP_004038_1255; c1) PSP_001440_1255; c2) PSP_001981_1255; c3) PSP_002337_1255; c4) PSP_002482_1255; c5) PSP_002548_1255; c6) PSP_003326_1255; d1) ESP_011580_1255; d2) ESP_012213_1255; d3) ESP_013136_1255; d4) ESP_020217_1255; d5) ESP_020784_1255; d6) ESP_021562_1255. HiRISE Image credits: NASA/JPL/University of Arizona. North is up in all images.

Figure 9. Active processes observed at the surface of the Russell Crater megadune as a function of solar longitude (L_s, see Table 1 for source images), each HiRISE image is marked with a hollow circle. (**a**) Timing of changes in perennial rills, where the first image with a change is marked with a cross. For each Mars Year the period between the first image with a change and the one preceding it is marked by a grey box – the darker the grey the greater the number of Mars Years. (**b**) Timing of dark spots and flows. The period where dark spots are observed in all Mars Years is shown with a light grey box and the period for which dark flows are seen in all Mars Years in a darker shade of grey. (**c**) The timing of presence of images with dust devil tracks are marked by filled circles, and the grey box marks continuous presence in all Mars Years (with the exception of one image in MY32). (**d**) A summary of all the observations, where a thick line marks the most probable timing given data from all Mars Years, the thin line possible timings based on data from individual Mars Years and a dotted line indicating presence of the features, yet conflicting data from different Mars Years. Note that although CO_2 ice is not detected in our data before Ls 120°, other datasets and models suggest that it should be present (e.g., Piqueux et al. 2015).

Figure 10. Hydrous mineralogy of the Russell Crater megadune. (**a**) CRISM mineral map of hydrous minerals on the Russell Crater megadune (in blue) over a CTX image. The footprint of

the CRISM observation is in dashed black lines. (**b**) CRISM spectra from the possible hydrous mineral outcrops and laboratory spectra for comparison. Two CRISM spectra are shown in black. Tentative laboratory matches are shown in colour: chloride hydrate (brown), opaline silica (green), the sulfate jarosite (blue), the sulfate bassanite (orange), the zeolite mordenite (purple) and an Al-rich smectite (red). Laboratory spectra originate from the RELAB spectral repository and Hanley et al. (2011). (**c**) HiRISE close-up of the area outlined by a dotted white line in panel (a) in the south-western part of the hydrous mineral exposure. The HiRISE, CTX and CRISM acquisitions were made on the same day.

Figure 11. Possible pits associated with perennial rills in MY28-32 in a-d compared to typical pits associated with activity in linear dune gullies (Pasquon et al. 2016) in MY30-32 e-g. Possible pits are identified by circles on the images a-d, but are too numerous to label for the linear dune gullies. In the a-d sequence MY31 is not shown because of poor image quality and MY33 because of frost deposits. All images are shown at the same scale as indicated in panel (a). HiRISE images: (**a**) PSP_003326_1255 (**b**) ESP_012213_1255 (**c**) ESP_020784_1255 (**d**) ESP_038335_1255 (**e**) ESP_020770_1300 (**f**) ESP_029038_1305 g) ESP_038255_1300. HiRISE Image credits: NASA/JPL/University of Arizona.

Figure 12. Channels with distributary patterns in their downstream sections, developing at the surface of a melting glacier in Iceland. (**a**) These channels are on Eyjabakkajökull, an outlet glacier that drains the northwestern margin of the Vatnajökull glacier, Iceland (64°39’57’’N, 15°41’54’’W). The dark region in the upper part of the picture comprises a surface slush layer that has developed by melting of the underlying massive and impermeable glacier ice, whereas the white region below comprises a layer of permeable (melting) firn covering massive and

impermeable glacier ice. (**b**) Zoom on the distal part of the channels, showing the frontal ice dams successively built at tips of each branch of the distributary pattern.

Figure 13. Scenario for the formation of a distributary channel network. (a) Meltwater produced during the warmer hours of the day triggers a first pulse (T_1). (b) The liquid fraction of the flow refreezes and/or ice particles build-up due to infiltration of the liquid at the end of the flow-front T_1. The older immobile deposits from flow (T_1) present a small topographic obstacle for the new flow (T_2), hence deflecting its path.

Figure 14. Loose wet snow avalanche on the eastern slopes of Mount Morrison in the Sierra National Forest, California. Image taken as part of the monitoring programme of the Eastern Sierra Avalanche Center on 11th March 2018. The avalanche was released on a ~40° slope from the snow in the rocky chutes, the snow balls (or roller balls) have rolled chaotically across the slope leaving trails behind them and do not necessarily follow the line of steepest decent. Source: http://www.esavalanche.org/content/loose-wet-avalanches-morrison-and-little-morrison

Table 1. Summary of *HiRISE images and CRISM hyperspectral data used in this study*

MY	HiRISE	CRISM	L_s	Acquisition date	Dark spots	Dark flows	Dust devil tracks	Bright halo	Perennial rills	CO_2 ice
28	PSP_001440_1255	MSW00003047	136.335	2006-Nov-16	X					X
28	PSP_001981_1255	FRT000039DF	157.704	2006-Dec-28	X					X
28	PSP_002337_1255	HRS00004006	172.628	2007-Jan-25	X	X				X
28	PSP_002482_1255	FRT000042AA	178.915	2007-Feb-05	X	X				X
28	PSP_002548_1255	HRS000043BC	181.817	2007-Feb-10	X	X	X			X
28	PSP_002904_1255		197.894	2007-Mar-10	X	X				
		FRT00005339	214.6	07/04/2007	-	-	-	-	-	X
28	PSP_003326_1255	MSW0000550B	217.794	2007-Apr-12			X	X	X	
28	PSP_003682_1250		235.118	2007-May-10			X			-
28	PSP_003748_1250		238.364	2007-May-15			X			-
28	PSP_004038_1255	FRT000061B2	252.689	2007-Jun-07			X			
28	PSP_004249_1255	FRT0000659F	263.109	2007-Jun-23			X			
28	PSP_005238_1255	FRT000078DF	310.265	2007-Sep-08			X			
28	PSP_005383_1255	FRT00007C73	316.793	2007-Sep-19			X			
28	PSP_005528_1255	FRT00007F9E	323.202	2007-Oct-01			X			
28	PSP_006161_1250		349.77	2007-Nov-19			X			-
29	PSP_006873_1255	FRT0000966B	17.18	2008-Jan-13						
29	PSP_007018_1255	MSW00009A0E	22.5	2008-Jan-25						
29	PSP_007229_1255		30.113	2008-Feb-10						-
29	PSP_007519_1255	FRT0000A3D5	40.368	2008-Mar-04						
29	PSP_009879_1255	FRT0000C55B	122.233	2008-Sep-04	X					X
29	PSP_010090_1255	MSP0000C9D3	130.055	2008-Sep-20	X					
29	PSP_010301_1255	FRT0000CD8E	138.06	2008-Oct-07	X					X
29	PSP_010446_1255	MSP0000CFE5	143.678	2008-Oct-18	X					
29	PSP_010868_1255	MSP0000D767	160.636	2008-Nov-20	X	X				
		FRT00010589	185.0	03/01/2009	-	-	-	-	-	
29	ESP_011580_1255	MSP00010873	191.503	2009-Jan-14	X	X				
29	ESP_012213_1255	MSP0001171F	221.24	2009-Mar-05			X	X	X	
29	ESP_012569_1255		238.638	2009-Apr-01			X			-
29	ESP_013136_1255	HRS00012B0D	266.636	2009-May-16			X			
30	ESP_017237_1255	FRT000179B1	71.342	2010-Mar-31						
30	ESP_018516_1255		115.721	2010-Jul-09	X					-
30	ESP_018872_1255	FRT0001A2D9	128.778	2010-Aug-06	X					
30	ESP_019083_1255		136.752	2010-Aug-22	X					-
30	ESP_019439_1255		150.671	2010-Sep-19	X					-
30	ESP_019650_1255		159.227	2010-Oct-05	X	X				-
30	ESP_019861_1255		168.028	2010-Oct-22	X	X				-
30	ESP_020217_1255		183.455	2010-Nov-18	X	X				-

30	ESP_020428_1255		192.942	2010-Dec-05	X	X	CLOUDS			-
30	ESP_020784_1255	FRT0001CAEC	209.487	2011-Jan-01			X	X	X	
30	ESP_021496_1255		244.086	2011-Feb-26			X			-
30	ESP_021562_1255		247.348	2011-Mar-03			X			-
30	ESP_021918_1255		264.934	2011-Mar-31			X			-
30	ESP_022340_1255		285.481	2011-May-03			X			-
31	ESP_025597_1255		55.79	2012-Jan-12			X			-
31	ESP_027364_1255		116.864	2012-May-28	X					-
31	ESP_028063_1255		143.076	2012-Jul-22	X		X			-
31	ESP_028208_1255		148.786	2012-Aug-02	X		X			-
31	ESP_028419_1255		157.29	2012-Aug-18	X		X			-
31	ESP_028630_1255		166.037	2012-Sep-04	X		X			-
31	ESP_028841_1255		175.037	2012-Sep-20	X	X	X			-
31	ESP_029263_1255		193.805	2012-Oct-23	X	X	X			-
31	ESP_029408_1255		200.483	2012-Nov-03	X	X	X			-
31	ESP_029619_1255		210.389	2012-Nov-20	-	-	CLOUDS	-	-	-
31	ESP_029764_1255		217.313	2012-Dec-01			X		X	-
31	ESP_029830_1255		220.492	2012-Dec-06			X			-
31	ESP_030120_1255		234.626	2012-Dec-29			X			-
31	ESP_030186_1255		237.872	2013-Jan-03			X			-
31	ESP_030542_1255		255.459	2013-Jan-31			X			-
31	ESP_030898_1255		272.975	2013-Feb-28			X			-
31	ESP_031755_1255		313.387	2013-May-05			X			-
31	ESP_032533_1255		346.696	2013-Jul-05			X			-
32	ESP_033456_1255		22.131	2013-Sep-15						-
32	ESP_034089_1255		44.613	2013-Nov-03			X			-
32	ESP_034234_1255		49.632	2013-Nov-15			X			-
32	ESP_034445_1255		56.879	2013-Dec-01			X			-
32	ESP_036357_1255		123.302	2014-Apr-29	X					-
32	ESP_037280_1255		159.117	2014-Jul-10	X					-
32	ESP_037702_1255		176.971	2014-Aug-12	X	X	X			-
32	ESP_038335_1255		205.645	2014-Sep-30			X	X	X	-
32	ESP_038467_1255		211.885	2014-Oct-10			X			-
32	ESP_038797_1255		227.793	2014-Nov-05						-
32	ESP_039153_1255		245.294	2014-Dec-03			X			-
32	ESP_039298_1255		252.466	2014-Dec-14			X			-
33	ESP_043267_1255		57.07	2015-Oct-19			X			-
33	ESP_044678_1255		105.484	2016-Feb-06						-
33	ESP_045377_1255		130.855	2016-Apr-01	X		X			-
33	ESP_045588_1255		138.878	2016-Apr-17	X		X			-
33	ESP_046089_1255		158.789	2016-May-26	X		X			-
33	ESP_046155_1255		161.511	2016-May-31	X					-
33	ESP_046511_1255		176.619	2016-Jun-28	X	X	X			-

33	ESP_046722_1255	185.918	2016-Jul-15	X	X	X			-
33	ESP_046867_1255	192.455	2016-Jul-26	X	X	X			-
33	ESP_047078_1255	202.175	2016-Aug-11	X	X	X	X	X	-
33	ESP_047434_1255	219.063	2016-Sep-08			X			-
33	ESP_047790_1255	236.42	2016-Oct-06			X			-
33	ESP_049148_1255	302.427	2017-Jan-20			X			-
33	ESP_049992_1255	339.563	2017-Mar-26			X			-
33	ESP_050203_1255	348.216	2017-Apr-12			X			-

The presence of each seasonal activity (dark spot, dark flow, dust devil tracks, bright halo, new perennial rills and CO_2) is marked as an "X" in the table for each line and "-" indicates no data (or no suitable data) available. Note that although CO2 ice is not detected in our data before Ls 120°, other datasets and models suggest that it should be present (e.g., Piqueux et al. 2015).

Table 2. *Activity of perennial rill zones per year*

Zone ID	MY28	MY29	MY30	MY31	MY32	MY33	Area (m^2)
1	X	X	X	X	X	X	56993
2			X	X	X	X	54839
3			X		X	X	36957
4	X	X	X		X	X	26610
5	ND				X	X	38487
6	ND	X			X	X	83907
7	ND				X	X	15884
8	ND				X	X	9729
9	ND				X	X	8006
10	ND		X		X	X	3422
11						X	2172
12						X	2490
13						X	2797
14			X		X	X	3946
15						X	1974
16	X	X	X	X			6521
17	X	X			X	X	4747
18	X				X	X	21334
19	X		X		X	X	6104
20		X	X		X	X	5117
21				ND	X	ND	2527
22			X		X		2016
23			X	ND	X		1353
24	X		X		X	X	3393
25					X		4548
26	X	X	X		X		7084
27	X		X		X		2853
28			X		X		2279
Surface area active per year (m^2)	135640	190980	219488	118354	402135	388909	
Number of sites active per year	9	7	15	3	23	20	

The ID refers to those marked on Fig. 4. “X” in any given MY=Mars Year column meaning that zone grew or changed during the previous year. “ND” indicates No Data (zone located outside HiRISE image extent) and blank means no activity noted. “Area” refers to the total active area over the whole observation period.

Figure 1 (jpg, tiff at link)

Click here to access/download;figure;Figure1_Context_sml.jpg

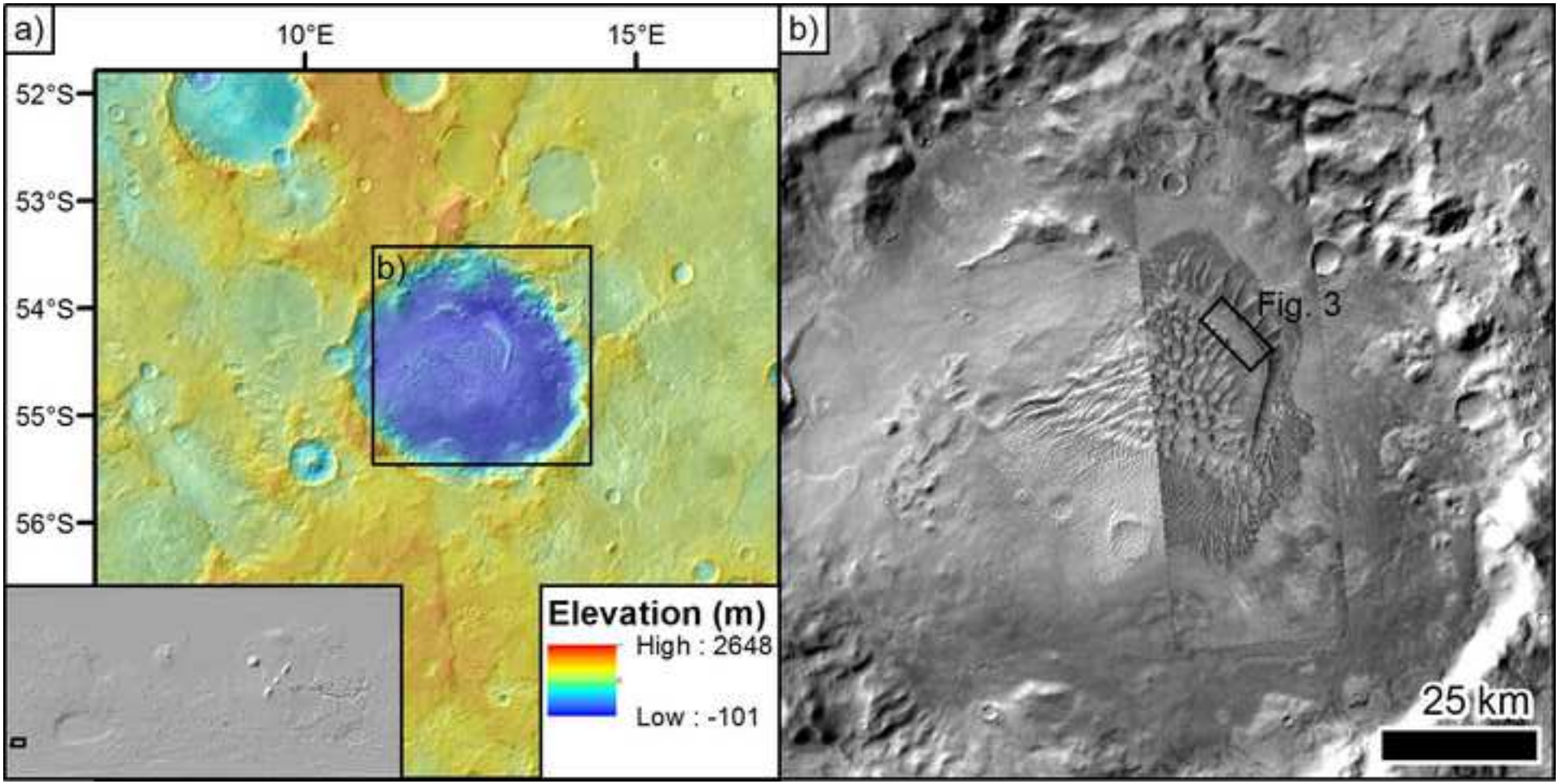

figure 2

Click here to access/download;figure;Figure02.tif

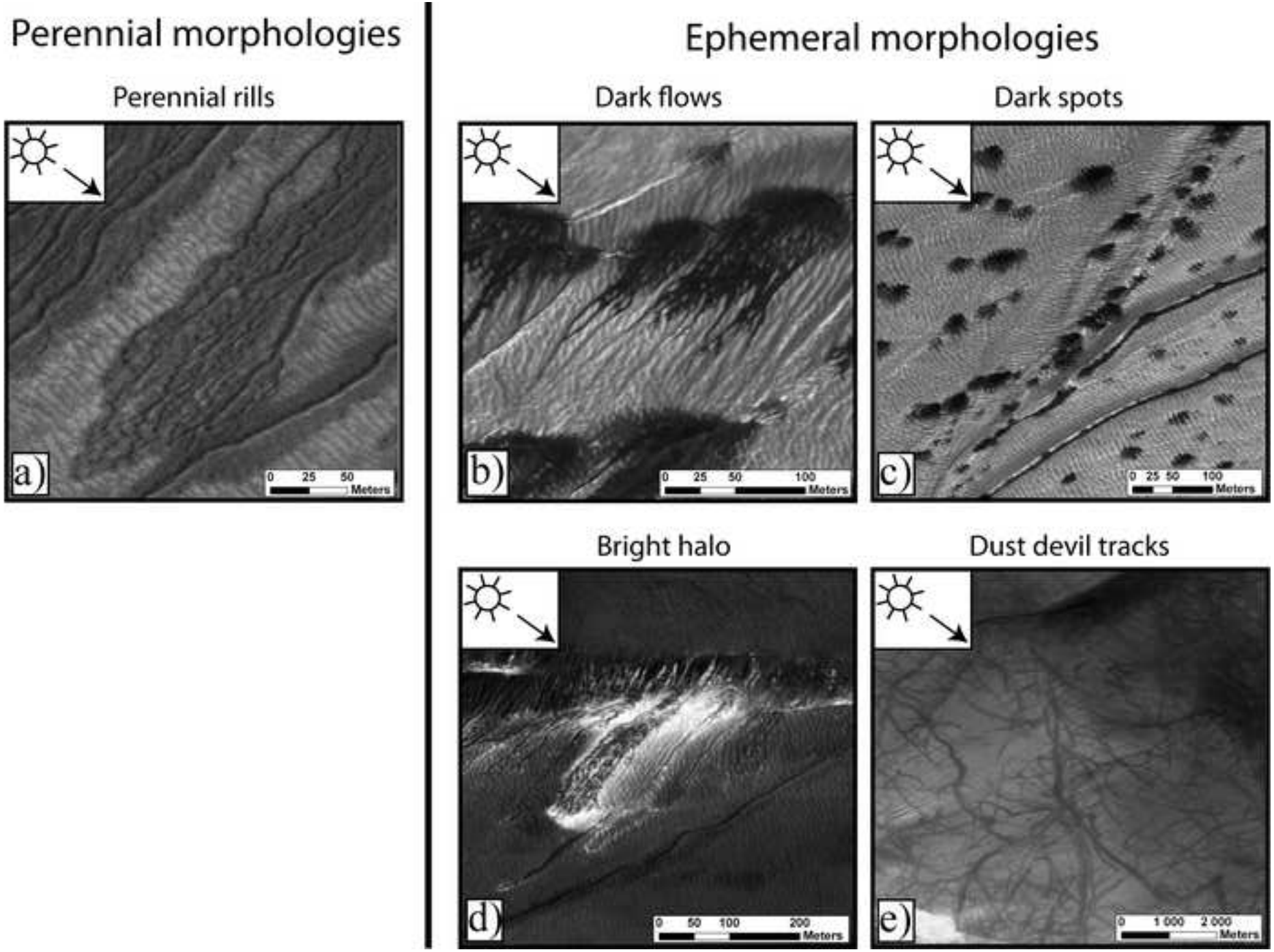

Figure 3 (jpg, tiff at link)

Click here to access/download;figure;Figure3_topoContext_sml.jpg

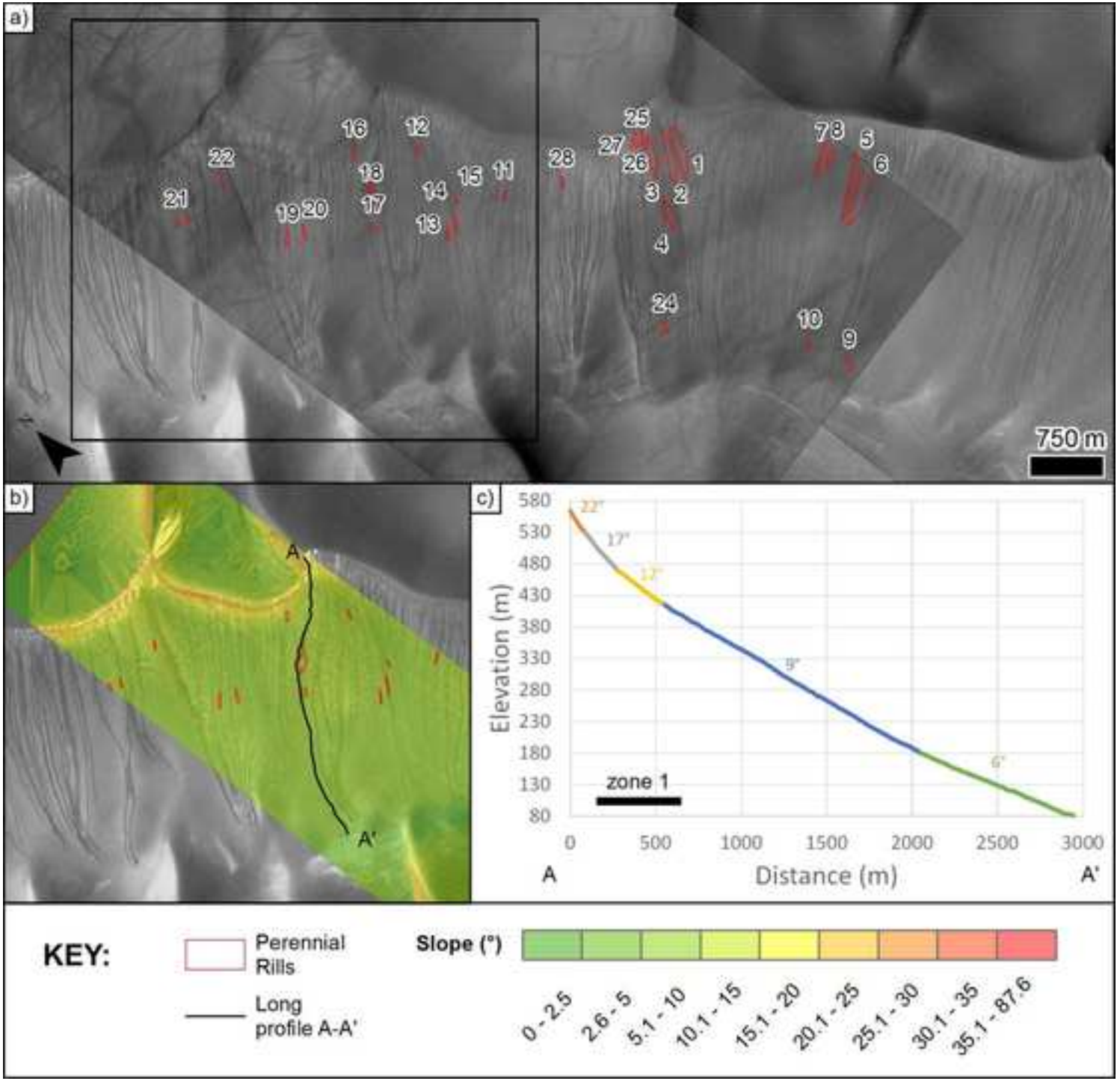

figure 4 (jpg, tiff at link)

Click here to access/download;figure;Figure04_sml.jpg

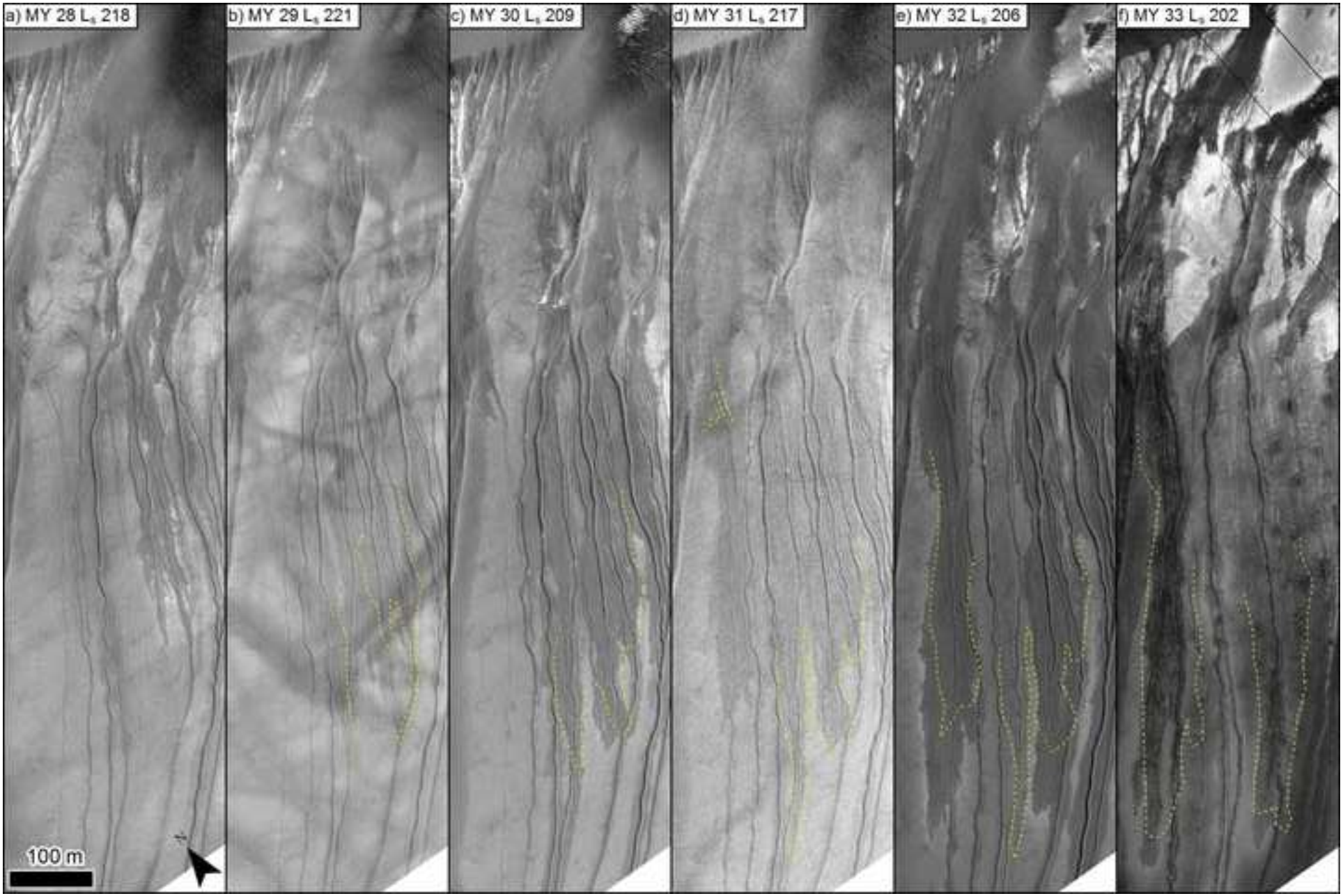

figure 5 (jpg, tiff at link)

Click here to access/download;figure;Figure05sml.jpg

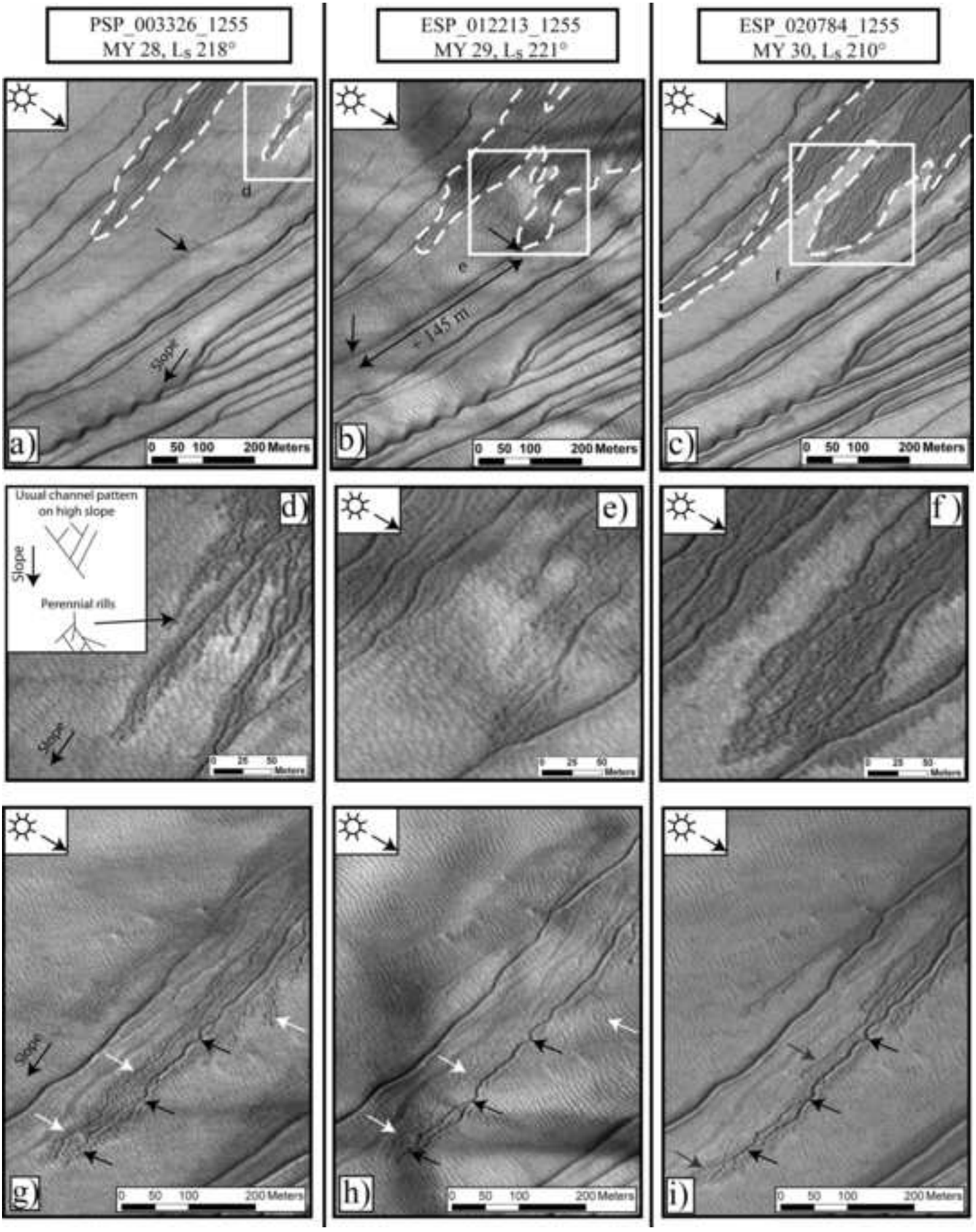

figure 6

Click here to access/download;figure;Figure06.tif

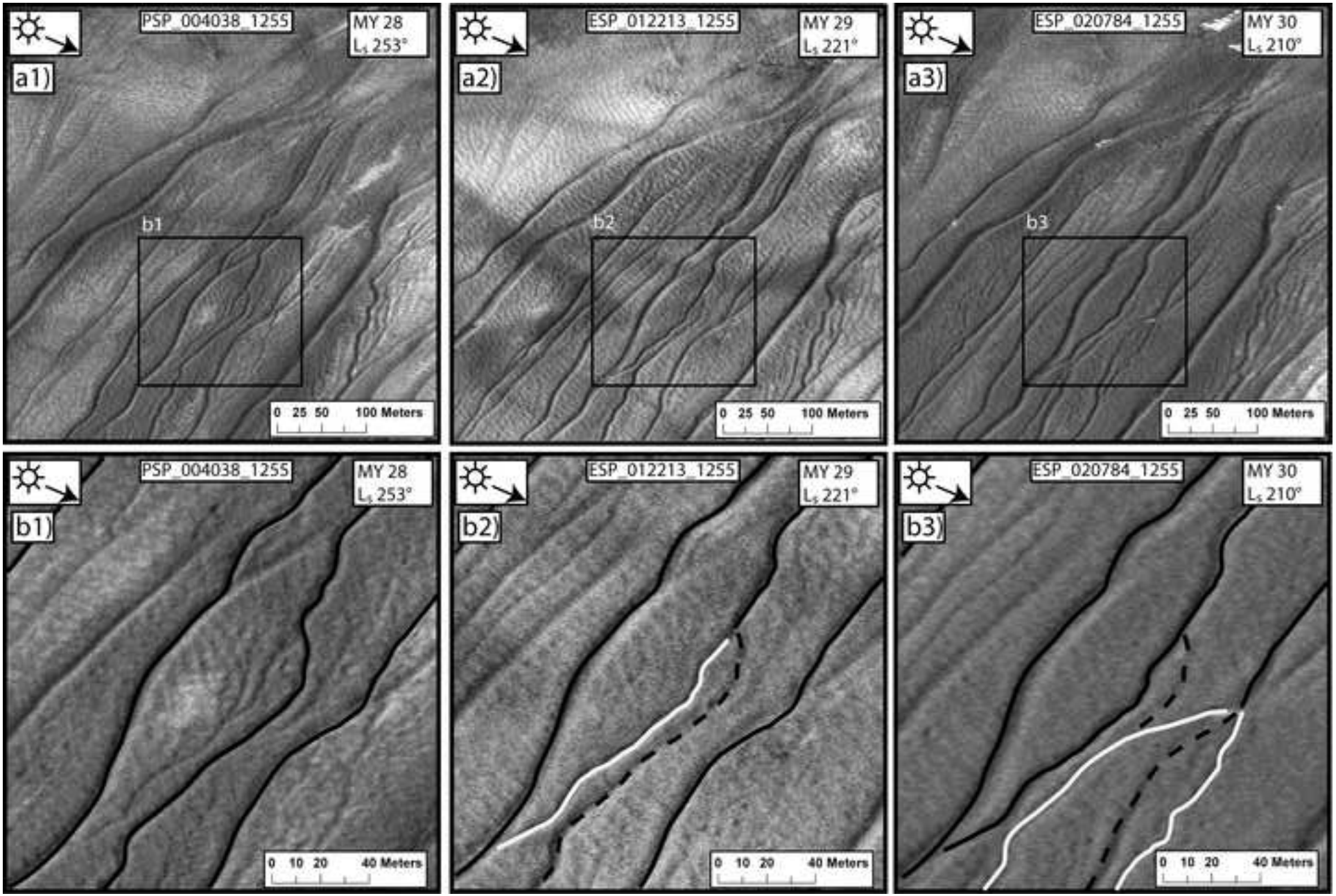

figure 7

Click here to access/download;figure;Figure07.eps

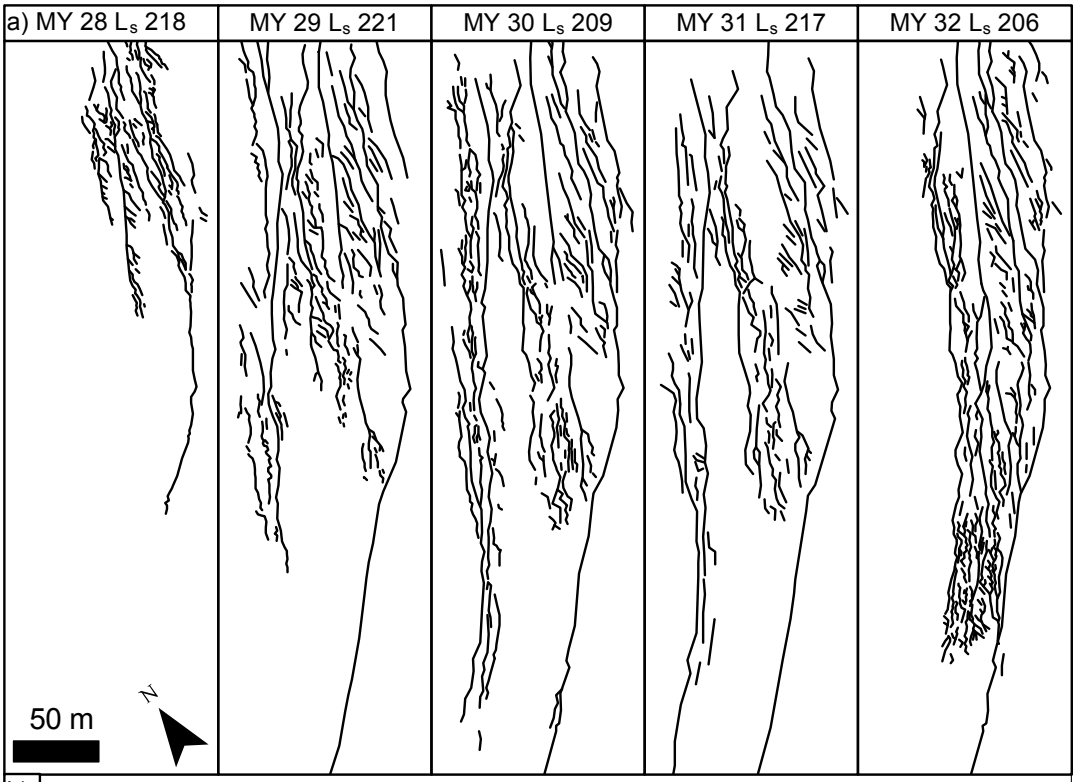

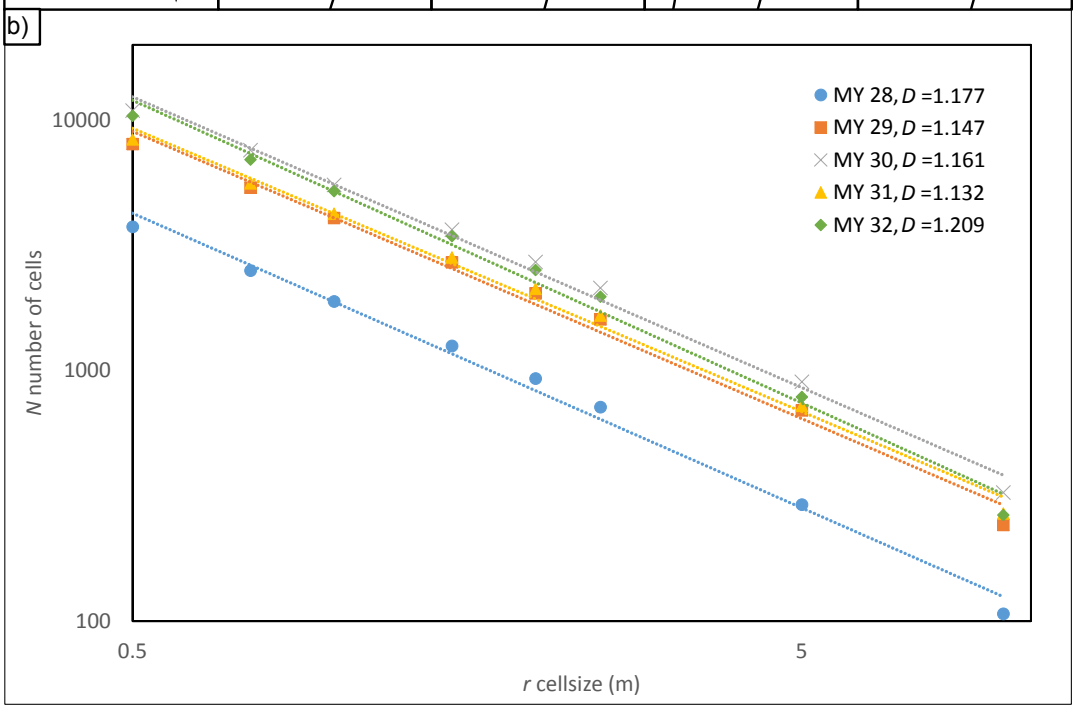

figure 8 (jpg, tiff at link)

Click here to access/download;figure;Figure08_sml.jpg

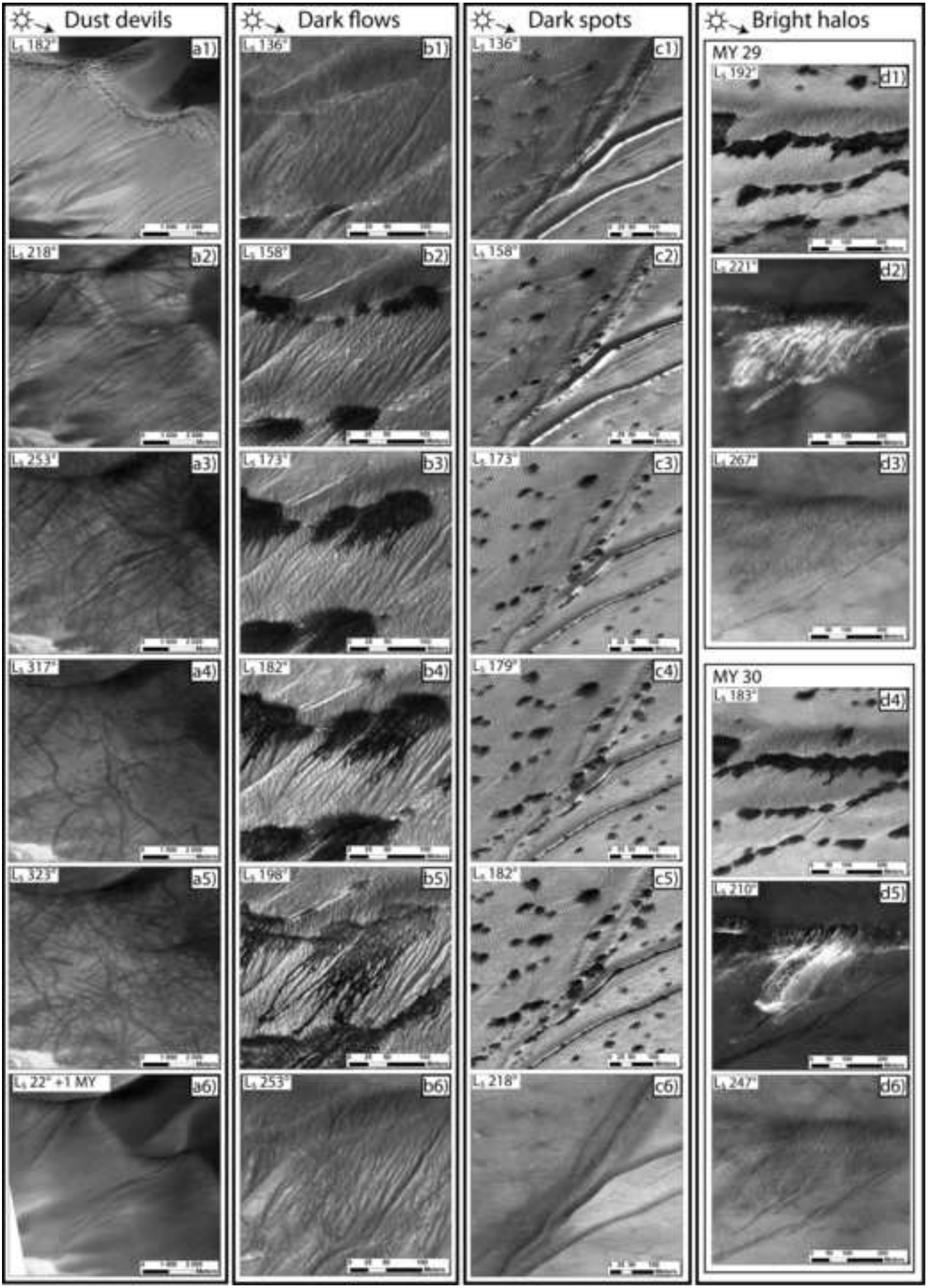

figure 9

Click here to access/download;figure;Figure09.eps

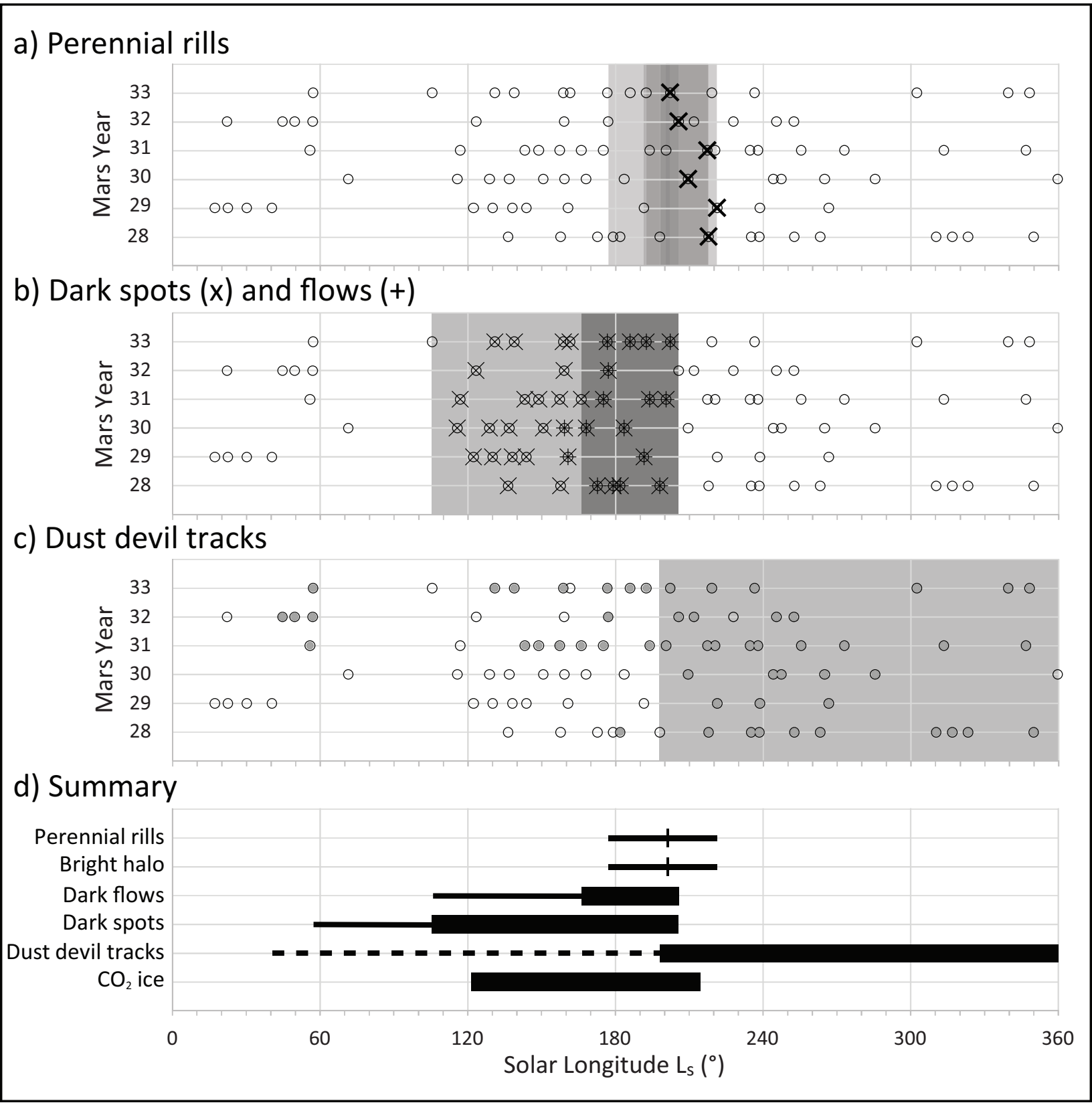

Figure 10 (jpg, higher res at link)

Click here to access/download;figure;Figure10_CRISM_sml.jpg

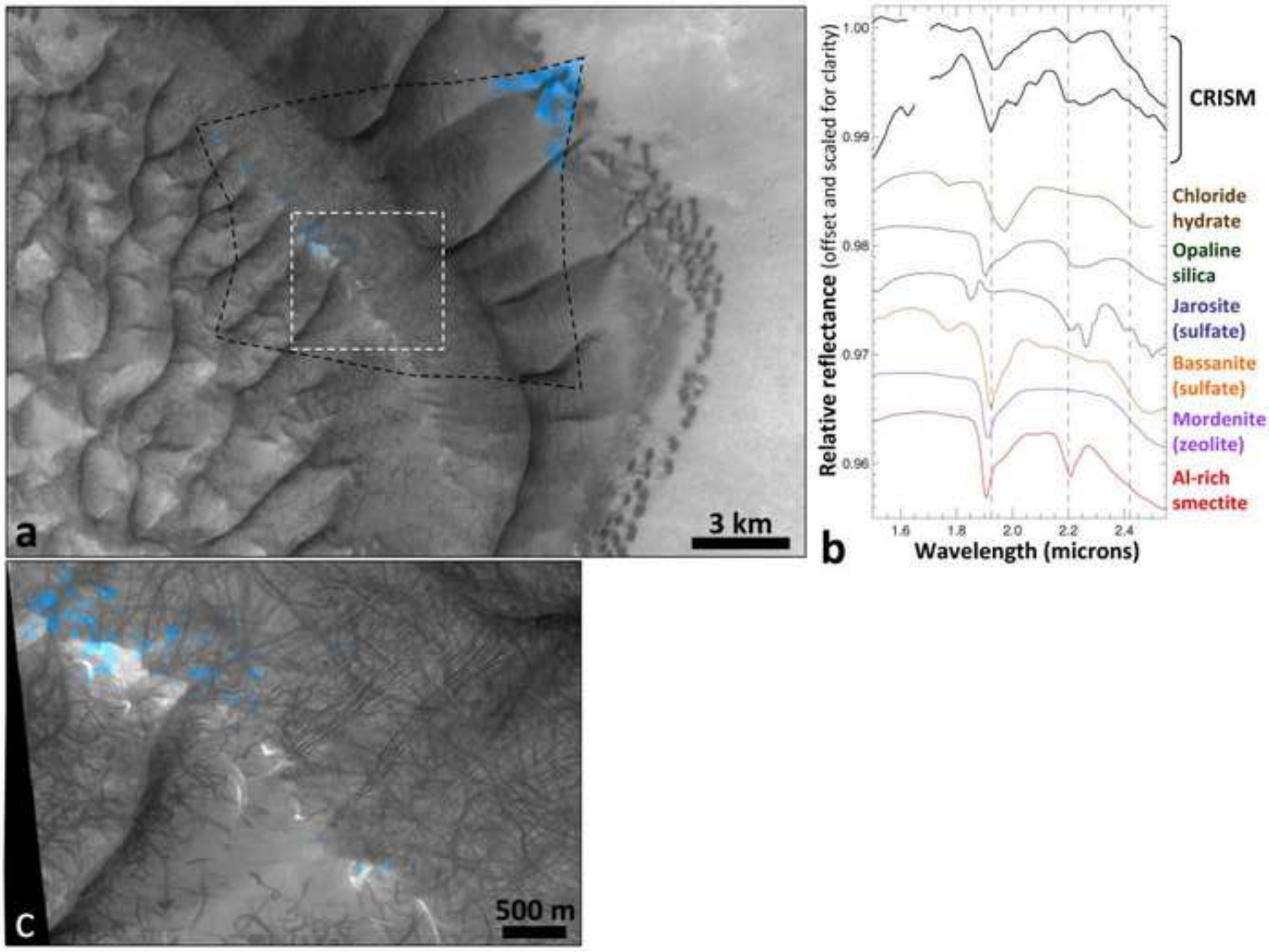

figure 11 (jpg, tiff at link)

Click here to access/download;figure;Figure11_sml.jpg

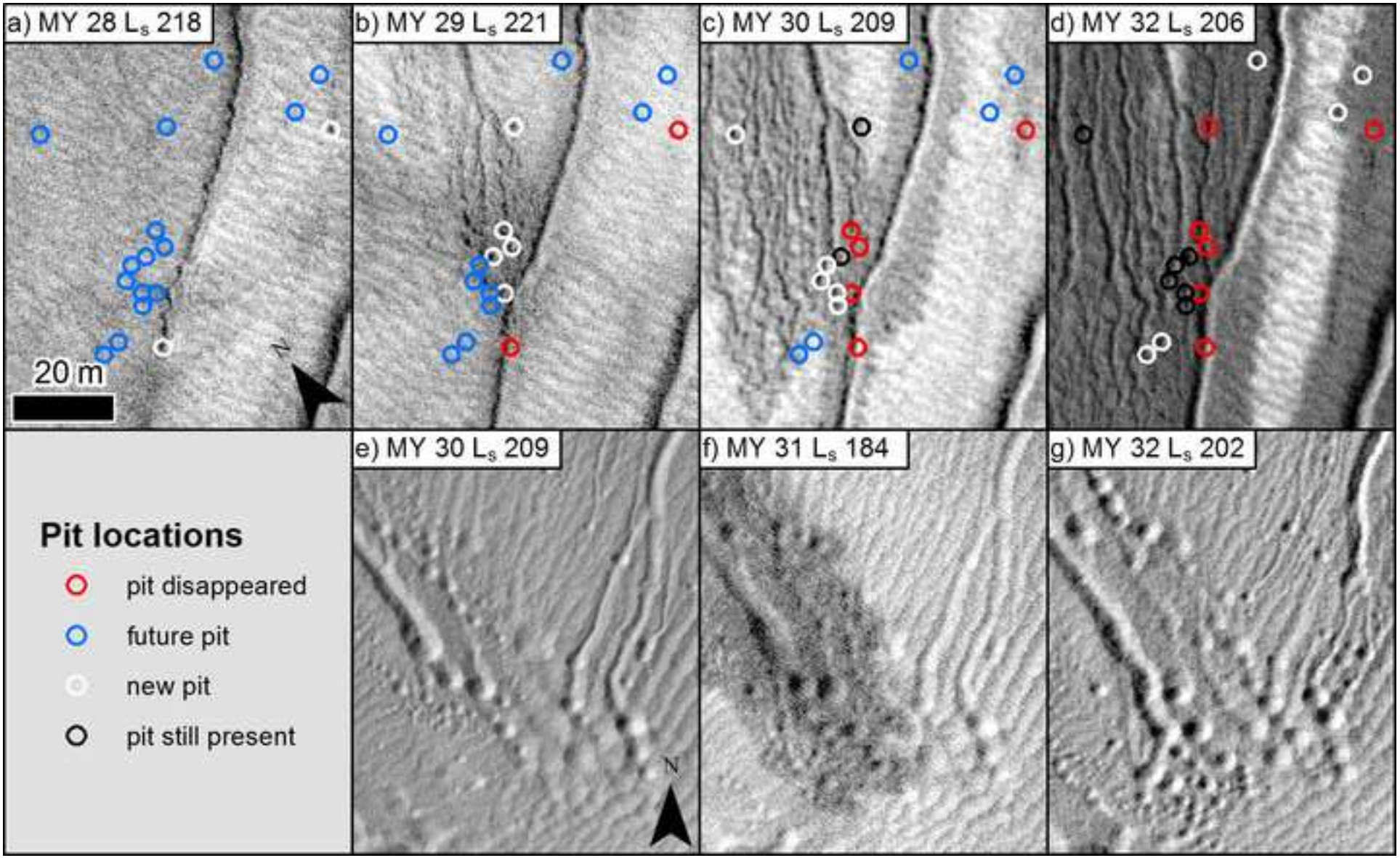

Figure 12 (jpg, tiff at link)

Click here to access/download;figure;Figure12_Iceland_sml.jpg

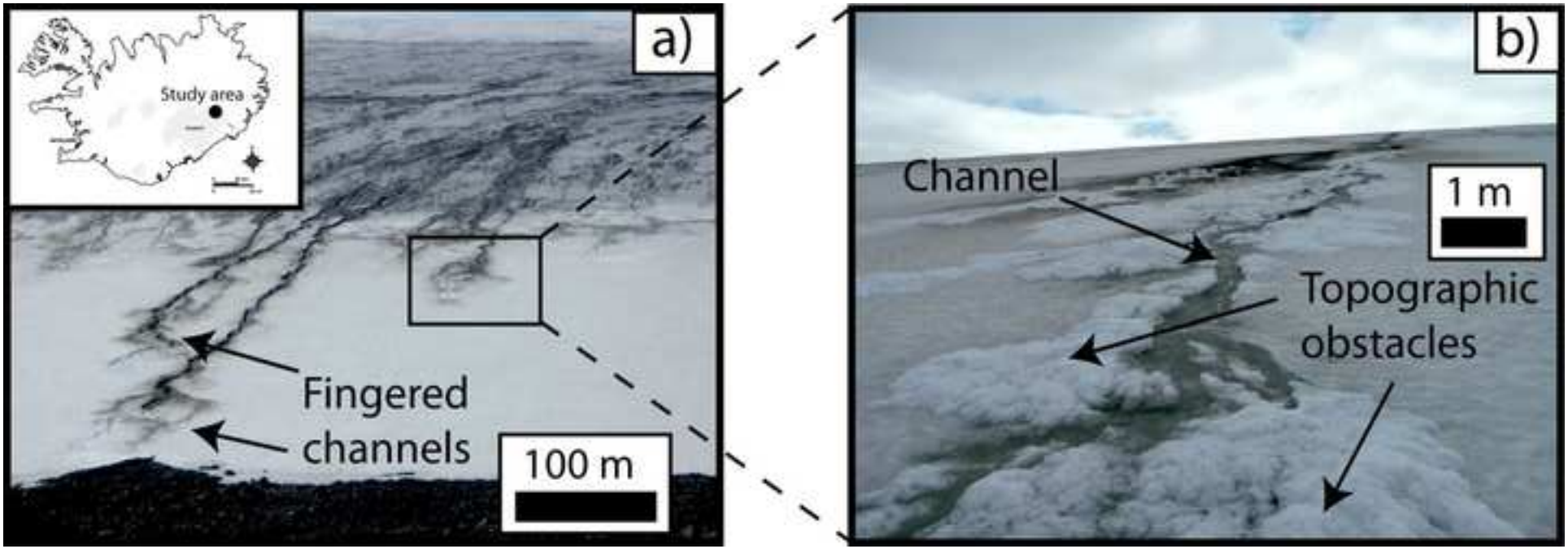

figure 13

Click here to access/download;figure;Figure13_unchanged.eps

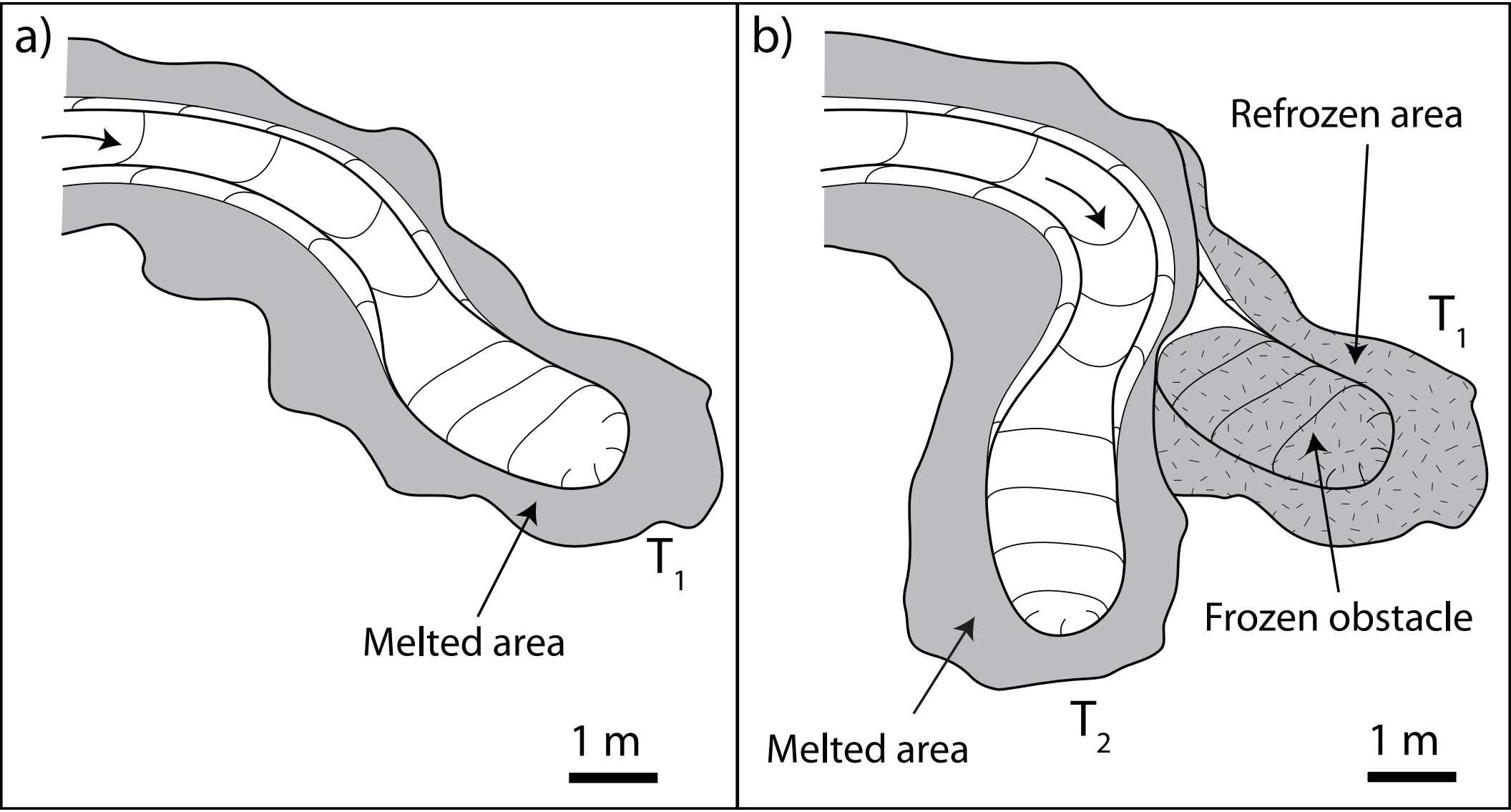

figure 14

Click here to access/download;figure;Figure14.jpg